The bifurcation of periodic orbits and equilibrium points in the linked restricted three-body problem with parameter ω

Cite as: Chaos **29**, 103110 (2019); https://doi.org/10.1063/1.5096966
Submitted: 21 March 2019 . Accepted: 16 September 2019 . Published Online: 08 October 2019

Yuying Liang, Jinjun Shan, Ming Xu, and Mingpei Lin

Chaos ARTICLE scitation.org/journal/cha

The bifurcation of periodic orbits and equilibrium points in the linked restricted three-body problem with parameter ω

Cite as: Chaos **29**, 103110 (2019); doi: 10.1063/1.5096966
Submitted: 21 March 2019 · Accepted: 16 September 2019 ·
Published Online: 8 October 2019

Yuying Liang,[1] Jinjun Shan,[1] Ming Xu,[2,a)] and Mingpei Lin[2]

AFFILIATIONS

[1]Department of Earth and Space Science and Engineering, York University, Toronto M3J 1P3, Canada
[2]School of Astronautics, Beihang University, Beijing 100191, China

[a)]**Email address:** xuming@buaa.edu.cn

ABSTRACT

This paper is devoted to the bifurcation of periodic orbits and libration points in the linked restricted three-body problem (LR3BP). Inherited from the classic circular restricted three-body problem (CR3BP), it retains most of the dynamical structure of CR3BP, while its dynamical flow is dominated by angular velocity ω and Jacobi energy C. Thus, for the first time, the influence of the angular velocity in the three-body problem is discussed in this paper based on ω-motivated and C-motivated bifurcation. The existence and collision of equilibrium points in the LR3BP are investigated analytically. The dynamic bifurcation of the LR3BP under angular velocity variation is obtained based on three typical kinds of periodic orbits, i.e., planar and vertical Lyapunov orbits and Halo orbits. More bifurcation points are supplemented to Doedel's results in the CR3BP for a global sketch of bifurcation families. For the first time, a new bifurcation phenomenon is discovered that as ω approaches to 1.4, two period-doubling bifurcation points along the Halo family merge together. It suggests that the number and the topological type of bifurcation points themselves can be altered when the system parameter varies in LR3BP. Thus, it is named as "bifurcation of bifurcation" or "secondary bifurcation" in this paper. At selected values of ω, the phase space structures of equilibrium points L_2 and L_3 are revealed by Lie series method numerically, presenting the center manifolds on the Poincaré section and detecting three patterns of evolution for center manifolds in LR3BP.

Holding the key to the origin of the universe, small bodies, e.g., asteroids are attracting more and more interest from academic and industrial fields. Current simulation on asteroid is implemented based on the regular spinning rate of an asteroid body. However, recently, the observation results on some asteroids show that their spinning velocity varies due to the solar radiation pressure, such as 2000 PH5, whose spinning velocity increases by $(2.0 \pm 0.2) \times 10^{-4}$°/day^2. The effect of the variable spinning velocity has not been fully understood. To cope with the orbital dynamics near a celestial object with varying angular velocity, a linked restricted three-body problem (LR3BP) is proposed in this paper given that the primary and the secondary are connected by a massless link. The bifurcations motivated by both angular velocity and Jacobi energy are detected to present the influence of the angular velocity. The expected results will provide new insights into orbital dynamics near asteroids, serving for future asteroid exploration mission. The LR3BP and the discovered bifurcation phenomena are important theoretical supplementation to the classic three-body problem theory.

I. INTRODUCTION

The purpose of the restricted three-body problem is to characterize the totality of possible motions of a given planetary system. The history of the restricted problem begins with Euler[1] and Lagrange.[2] Furtherly given the circular motion of the primary and the secondary, the circular restricted three-body problem (CR3BP) is proposed to formularize the general motion of a spacecraft in the gravity field for any planet and moon in the solar system. So far, there are abundant academic results on many topics of CR3BP, e.g., libration point orbits,[3] heteroclinic connections in interplanetary systems,[4] space manifolds,[5] chaotic motion,[6] resonance orbits,[7] and third-body perturbation.[8] Some have been successfully applied

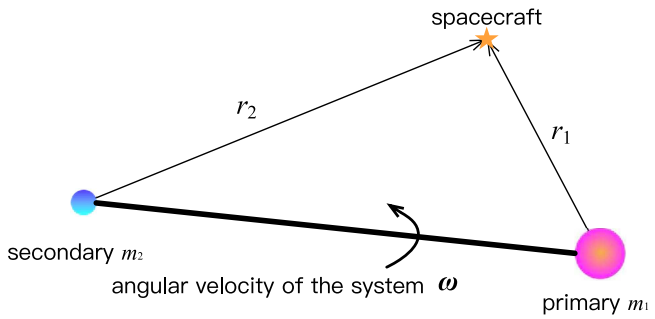

FIG. 1. The configuration of LR3BP.

to engineering missions, such as the Grail mission,[9] the rescue of Hiten.[10]

According to Kepler's third law,[11] the distance between the primary and the secondary in CR3BP, denoted by r, and the system's angular velocity ω obey the rule that $r^3\omega^2 = 1$. Since in most of the planet-moon systems, their distance remains the same with ignorable small variation in hundreds of years, so their angular velocity ω is nearly constant and can be regarded as 1 by certain normalization. Such a case has been thoroughly explored in most of the existing literature on celestial mechanics and astrodynamics.

However, recently, the observation results on some asteroids show that their spinning velocity varies due to the solar radiation pressure, such as 2000 PH5, whose spinning velocity increases by $(2.0 \pm 0.2) \times 10^{-4}$°/day^2.[12] Current simulation on asteroid is implemented based on the regular spinning rate of the asteroid body. The effect of the variable spinning velocity has not been fully understood.

To cope with the orbital dynamics near a celestial object with varying angular velocity ω, a linked restricted three-body problem (LR3BP) is proposed in this paper. In LR3BP, the primary and the secondary are physically connected by a massless link so that

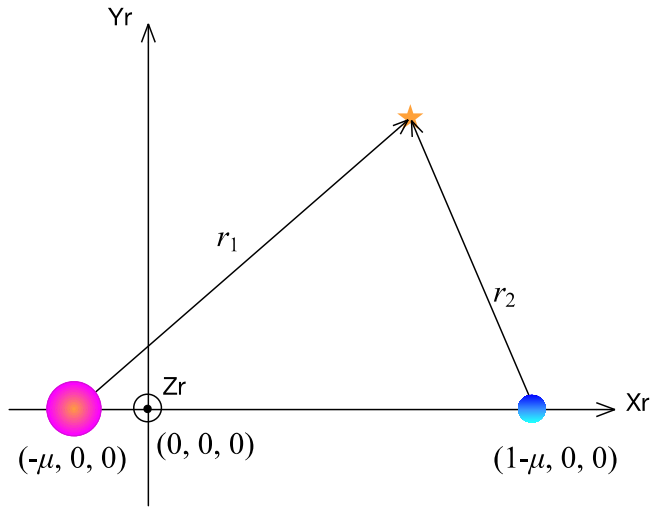

FIG. 2. The location of the primary and secondary in the rotating frame: the pink and blue marks indicate the primary and the secondary; the yellow star indicates the spacecraft; the z axis comes outwards the paper from the origin.

the distance between them is fixed, as shown in Fig. 1. Thus, the parameter ω can be explicitly expressed in the dynamical equations as

$$\begin{cases} \ddot{x} - 2\omega\dot{y} = \Omega_x, \\ \ddot{y} + 2\omega\dot{x} = \Omega_y, \\ \ddot{z} = \Omega_z, \end{cases} \tag{1}$$

where Ω indicates the effective potential. The detailed definition of each variable is shown in Sec. II. As an independent parameter, ω affects the dynamics of LR3BP. In this case, the inner property of dynamics in the LR3BP is essentially dominated by three parameters, i.e., the angular velocity ω, the mass ratio μ, and the Jacobi energy C.

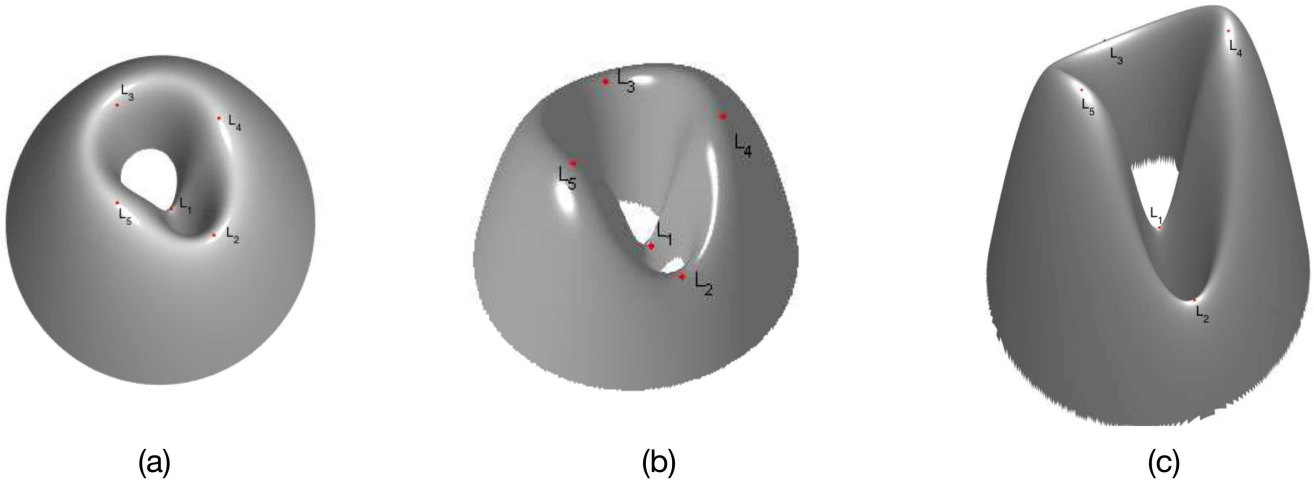

FIG. 3. The effective potential of LR3BP at μ=0.3, $\omega = 0.7$ (a), $\omega = 1.0$ (b), and $\omega = 1.2$ (c): five EPs are indicated by red dots.

TABLE I. The coordinate of EPs at $\omega = 1$.

No. EP	x coordinate	y coordinate
2	1.2474	0
3	−1.1390	0
4	0.1600	0.8660

The effect of μ on the dynamics of the CR3BP has been discussed in a lot of literature.[13,14] Therefore, the research on the dynamics of LR3BP with varying ω is a very important supplement to the classic three-body problem theory mathematically. Furthermore, the expected results related to LR3BP will provide new insights into orbital dynamics near asteroids, especially those binary contact asteroids, because it captures their main characters, such as mass distribution and spin rate.

Compared with the classic CR3BP, the interest in the LR3BP has been revived since 1980s. Chermnykh began the study of the Lyapunov stability of the triangular solutions in 1987.[15] Goździewski and Maciejewsky investigated Lyapunov stability of libration points in detail in the whole range of parameters ω and μ based on a rotating dumb-bell model.[16] Papadakis gave the analytical expression of periodic orbits of collinear libration points for different values of ω and of the coordinates of libration points.[17] Perdios and Ragos studied the nonsymmetric asymptotic motion to the collinear equilibrium points (EPs) and discussed their relation to families of symmetric periodic solutions.[18] Recently, many researchers are devoted to the dynamics in the asteroid's model with varying spinning velocities, such as Wang *et al.*,[19] and Jiang *et al.*[20,21] In particular, Ref. 16 gave a global distribution of (μ, ω) pair related to the linear stability of triangular libration points and discussed their nonlinear stability in resonance cases by the Kolmogorov–Arnold–Moser theorem. However, the bifurcation of periodic orbits and the bifurcation motivated by the Jacobi energy C remain an open question.

Therefore, this paper systematically studies the bifurcation of periodic orbits and libration points in the context of LR3BP. For the first time, the bifurcation phenomenon in the dynamics of LR3BP is discussed in two dimensions, i.e., the angular velocity ω and the Jacobi energy C. By the Lie series method, the dynamical behaviors before and after the bifurcation are manifested on the Poincaré section in the context of LR3BP. The discovered bifurcated families are supplemented to the result of Doedel *et al.*[22,23] establishing a global "skeleton" of LR3BP.

The Lie series method is first enlarged to encompass the cases where the generating function itself depends explicitly on the small parameter by Deprit.[24] Then, it is introduced to CR3BP by Jorba and Masdemont to the accurate description of the dynamical structure

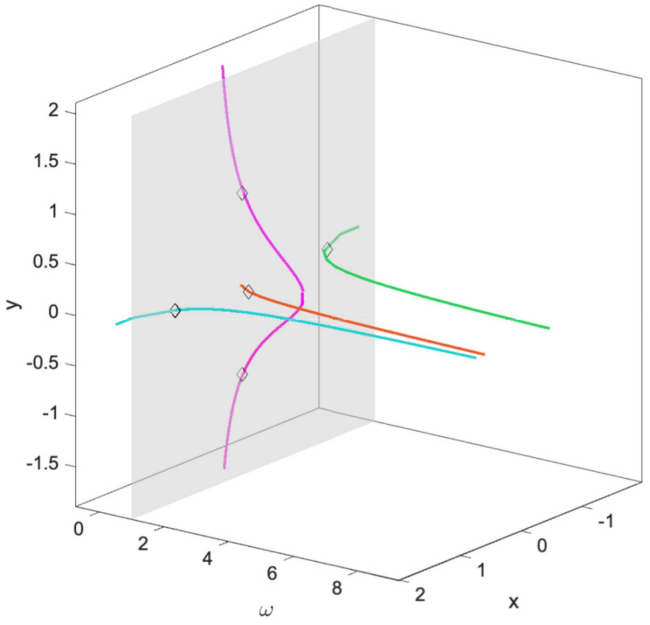

FIG. 4. The coordinate history of EPs L_1 (orange), L_2 (blue), L_3 (green), L_4 (upper segment in pink), and L_5 (lower segment in pink) as ω varies: the diamond indicates the coordinate of EPs at $\omega = 1$.

near collinear libration points, and the Hopf bifurcation from the Halo orbit family is first revealed.[25] Then, the bifurcation points along the family of libration point orbits are obtained by Gómez and Mondelo[26] with the bifurcated orbit families refined by the Lie series method with higher orders. The computation of the stable and unstable manifolds of libration point orbits in series expansions is accomplished by both the Lie series method and the Lindstedt–Poincaré method, which complement each other from a geometrical point of view.[26] Recently, Luo *et al.* applied the Lie series method to the dynamics of solar sail and proposed a high-order approximation of motion near the center point.[27] Following the idea of Jorba *et al.*, the Lie series method is employed in this paper to reduce the hyperbolic motion near the collinear libration points and demonstrate the new bifurcation phenomenon in dimensions of ω and C.

This paper is organized as follows: a brief introduction to the LR3BP model and its mathematical background is given in Sec. II. In Sec. III, the static bifurcation of the dynamical system in the context of LR3BP is studied both in analytical and numerical means including the existence and the collision of the EPs, and their topological type. Section IV focuses on the dynamical bifurcation phenomenon

TABLE II. The eigenvalues and stability of EPs at $\omega = 1$.

No. EP	λ_1	λ_1'	λ_2	λ_2'	Linear stability
2	1.3820	−1.3820	1.4378i	−1.4378i	Unstable
3	0.9295	−0.9295	1.2294i	−1.2294i	Unstable
4	$-0.6045 + 0.9303i$	$-0.6045 - 0.9303i$	$0.6045 + 0.9303i$	$0.6045 - 0.9303i$	Unstable

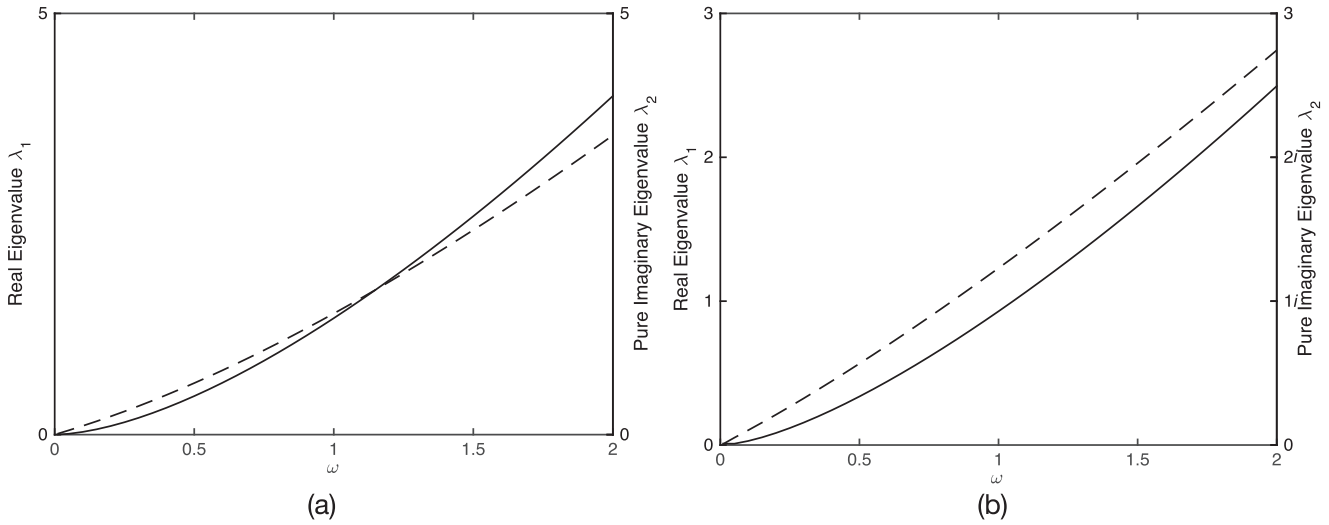

FIG. 5. The eigenvalue history of L_2 (a) and L_3 (b) at ω varies: the solid and dashed lines indicate the history of real eigenvalue and pure imaginary eigenvalue, respectively.

of the LR3BP, searching for bifurcation points and the associated bifurcated family by continuation along the libration periodic orbit family as ω varies. These bifurcated families are supplemented to the results of Doedel *et al.*,[22,23] establishing a global diagram of periodic orbit families in LR3BP. In Sec. V, the dynamical flow near the EPs of LR3BP is reduced to the center manifolds by the Lie series method as C varies, revealing the dynamical behavior change before and after the bifurcation.

II. LINKED THREE-BODY PROBLEM

In this paper, based on the classic CR3BP, a new dynamical model, called linked three-body problem (LR3BP) is proposed, where the primary is physically connected to the secondary by a massless link. The distance between the primary and the secondary is fixed due to the existence of the physical link even though the angular velocity varies. In this case, an extra tensile force (the angular velocity decreases) or compression force (the angular velocity increases) is

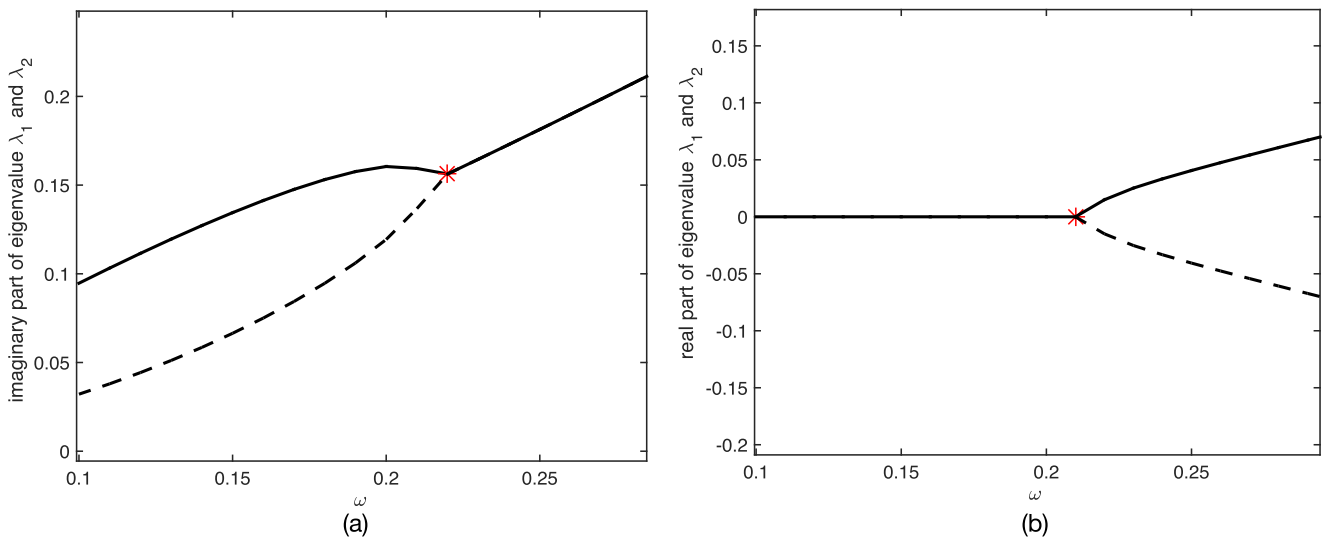

FIG. 6. The eigenvalue history of L_4 as ω varies: the solid and dashed lines indicate the eigenvalue history of λ_1 and λ_2, respectively; the red mark indicates a pitch-fork bifurcation at $\omega \approx 0.2131$.

provided by the link. Hence, the parameter ω of the dynamical system can be explicitly expressed in the dynamical equations as follows:

$$\begin{cases} \ddot{x} - 2\omega\dot{y} = \Omega_x, \\ \ddot{y} + 2\omega\dot{x} = \Omega_y, \\ \ddot{z} = \Omega_z. \end{cases} \tag{2}$$

Equation (2) describes the motion of a massless particle, i.e., spacecraft moving in the primary-secondary rotating frame of LR3BP, wherein, (x, y, z) denotes the coordinate of the spacecraft and $\Omega = \omega^2(x^2 + y^2)/2 + (1-\mu)/r_1 + \mu/r_2$ denotes the effective potential.

As shown in Fig. 2, let Xr–Yr–Zr be a rotating frame with the origin at the barycenter of the primary and secondary system. The x axis is coincident with the primary-secondary line and positive in the direction from the primary to the secondary. The y axis is positive in the direction of the secondary's velocity. The z axis is determined by the right-hand law. The coordinate of the primary body is $(-\mu, 0, 0)$, and the coordinate of the secondary body is $(1-\mu, 0, 0)$. The mass ratio is $\mu = m_1/(m_1 + m_2)$, where m_1 and m_2 represent the mass of the primary and secondary body, respectively. Ω_x, Ω_y, and Ω_z represent the first-order partial derivation of Ω along x, y, and z directions, respectively. The distance from the spacecraft to the primary and the secondary is denoted by r_1 and r_2, respectively, and $r_1 = \sqrt{(x+\mu)^2 + y^2 + z^2}$ and $r_2 = \sqrt{(x-1+\mu)^2 + y^2 + z^2}$. Most of the variables are inherited from the classic CR3BP and more details can be found in Ref. 11. Another important system parameter is Jacobi energy C, which satisfies $C = \omega^2(\dot{x}^2 + \dot{y}^2) + \dot{z}^2 - 2\Omega$. The corresponding Hamiltonian function $\mathcal{H}$ can be expressed as $\mathcal{H} = \frac{1}{2}(p_x + \omega y)^2 + \frac{1}{2}(p_y - \omega x)^2 + \frac{1}{2}p_z^2 - \Omega$.

As an independent parameter, ω will directly affect the property of the dynamical system. It is important to note that the normalization of the length and mass is the same as the one in CR3BP, while it changes for the angular velocity ω. The total mass of the primary and the secondary is normalized to 1, the distance between them is normalized to 1, and the period of the secondary moving around the primary at a selected reference state is normalized to 2π. Thus, the unit 1 of the angular velocity is taken as the value at the reference state. The dimensionless value of the angular velocity indicates the ratio between the associated real value and the reference one. As $\omega = 1$, LR3BP degenerates to normal CR3BP.

We compare Eq. (2) with the following dynamical equations of CR3BP:

$$\begin{cases} \ddot{x} - 2\dot{y} = \Omega_x, \\ \ddot{y} + 2\dot{x} = \Omega_y, \\ \ddot{z} = \Omega_z. \end{cases} \tag{3}$$

Both the Coriolis term and the effective potential term are changed when the LR3BP is introduced to describe the motion. Figure 3 demonstrates the influence of the angular velocity on the effective potential at $\mu = 0.3$, $\omega = 0.7$ (a), $\omega = 1.0$ (b), and $\omega = 1.2$ (c), respectively. Such conclusions can be drawn that in these three cases, there still exist five EPs as in CR3BP, denoted by L_i $(i = 1, 2, 3, 4, 5)$; the effective potential at L_1 decreases quickly with the reduction in ω while the value at L_2 decreases rapidly as ω increases. Although

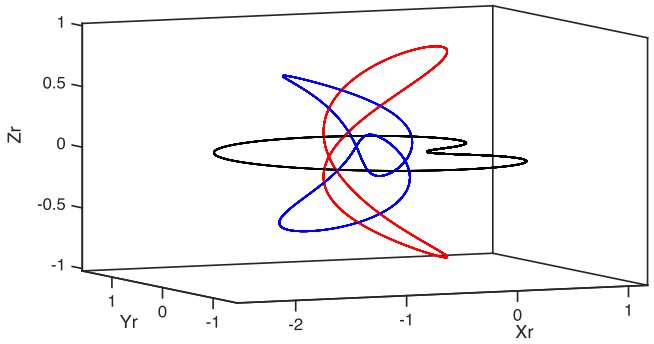

FIG. 7. North and South Halo orbits (blue), planar (black) and vertical (red) Lyapunov orbits of L_3 in the CR3BP at $\mu = 0.34$ and $\omega = 1$.

the collinear EPs are located at the saddle point on the energy surface geometrically with their topological structure unchanged, the dramatic change in the effective potential must affect the dynamical behavior in their neighborhoods. In the following sections, the EP L_1 is not studied since it is located under the surface of the celestial body due to the existence of the link. Note that besides the effective potential, LR3BP also inherits other properties of CR3BP, such as the symmetry with respect to the z axis and time and the autonomy of the dynamical system.

From the mathematical viewpoint, after being explicitly expressed in the dynamical equations, the parameter ω can exert an important influence directly on the dynamical flow of LR3BP, which will be demonstrated in the following sections. The research on this topic can be regarded as a significant supplement to the classic three-body problem theory. Furthermore, the LR3BP can also be used to approximate the gravity field of a contact binary asteroid system. They represent a special kind of asteroid system consisting of two objects, either ellipsoid or sphere being physical contact with each other, such as 1996 HW1.[28] Although the gravity field of a contact binary asteroid is simplified by the LR3BP, it still captures their main characteristics, e.g., mass distribution and rotation velocity. Based on the LR3BP, more complicated dynamical models of contact binary asteroids can be developed further considering the irregular shape of the primary and the secondary of the binary system or the mass of the link. In the following sections, the mass ratio μ is taken as the value of the contact binary asteroid 1996 HW1 and $\mu = 0.34$.[28]

III. BIFURCATION OF EQUILIBRIUM POINTS IN LR3BP

The EPs are essentially the gravitational equilibria in celestial mechanics, where a spacecraft is able to maintain stationarity with respect to the primary and the secondary without fuel consumption. Their coordinate can be obtained by solving the dynamical equations numerically, as listed in Table I. At $\omega = 1$, there exist four EPs in LR3BP. All of them are located on the x–y plane and two located on the line between the primary and the secondary are called collinear EPs. The others are located off the x axis in a configuration of equilateral triangle with the primary and the secondary and called triangular EPs. The collinear EPs are similar to the L_2 and L_3 in CR3BP, while L_1 disappears due to the existence of the link.

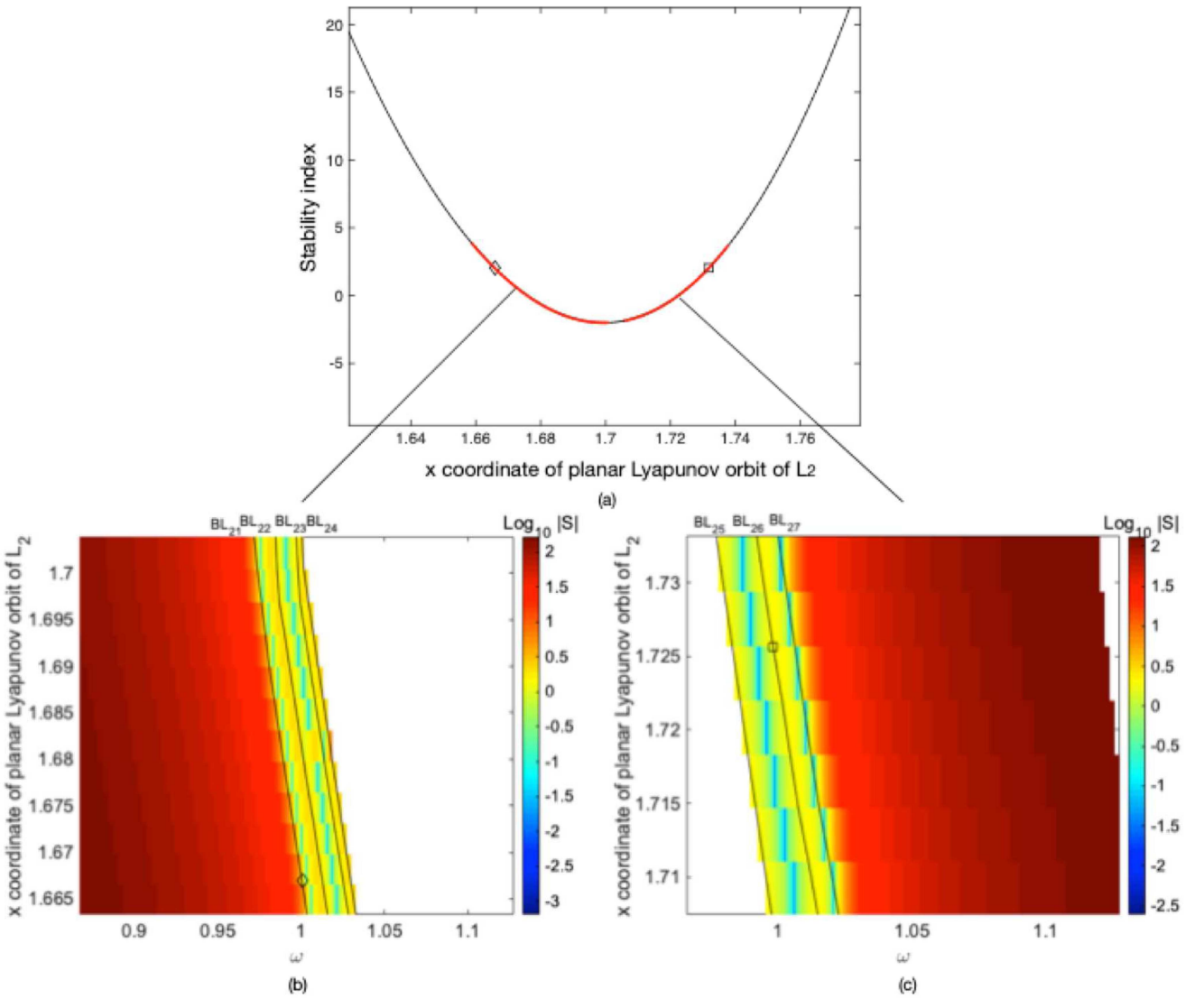

FIG. 8. The bifurcation of the planar Lyapunov orbit family of L_2 as ω varies.

In order to analyze the topological type of these four EPs, the dynamical equations are linearized with respect to the EP as

$$\begin{cases} \ddot{\tilde{x}} = 2\omega\dot{\tilde{y}} + \Omega_{\tilde{x}\tilde{x}}\tilde{x} + \Omega_{\tilde{x}\tilde{y}}\tilde{y}, \\ \ddot{\tilde{y}} = -2\omega\dot{\tilde{x}} + \Omega_{\tilde{y}\tilde{x}}\tilde{x} + \Omega_{\tilde{y}\tilde{y}}\tilde{y}, \end{cases} \tag{4}$$

where $\Omega_{\tilde{x}\tilde{y}}$ denotes the second-order partial derivative with respect to $\tilde{x}$ and $\tilde{y}$. By Equation (4), the motion along the z axis is independent of the one on the $x-y$ plane with no explicitly expressed ω involved. Hence, the variation of ω does not affect the topological behavior along the z axis, and the EPs L_i $(i=2,3,4,5)$ are always of the center type along that direction. Therefore, the dynamical behavior along the z axis including the associated eigenvalue and the topological type is not explored in this section.

We rewrite Eq. (4) into the following matrix form as

$$\begin{pmatrix} \dot{\tilde{x}} \\ \dot{\tilde{y}} \\ \ddot{\tilde{x}} \\ \ddot{\tilde{y}} \end{pmatrix} = \begin{pmatrix} 0 & 0 & 1 & 0 \\ 0 & 0 & 0 & 1 \\ -\Omega_{\tilde{x}\tilde{x}} & -\Omega_{\tilde{x}\tilde{y}} & 0 & 2\omega \\ -\Omega_{\tilde{x}\tilde{y}} & -\Omega_{\tilde{y}\tilde{y}} & -2\omega & 0 \end{pmatrix} \begin{pmatrix} \tilde{x} \\ \tilde{y} \\ \dot{\tilde{x}} \\ \dot{\tilde{y}} \end{pmatrix} = \boldsymbol{M} \begin{pmatrix} \tilde{x} \\ \tilde{y} \\ \dot{\tilde{x}} \\ \dot{\tilde{y}} \end{pmatrix}. \tag{5}$$

A preliminary study on the topological type and the phase space structure of the EPs is accomplished by analyzing the distribution of eigenvalues of the matrix $\boldsymbol{M}$, as listed in Table II.

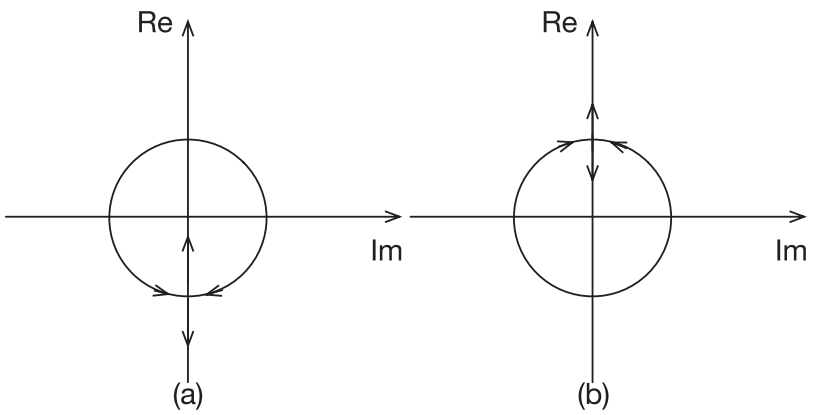

FIG. 9. The routine of eigenvalues across BL_{22} (a) and BL_{25} (b).

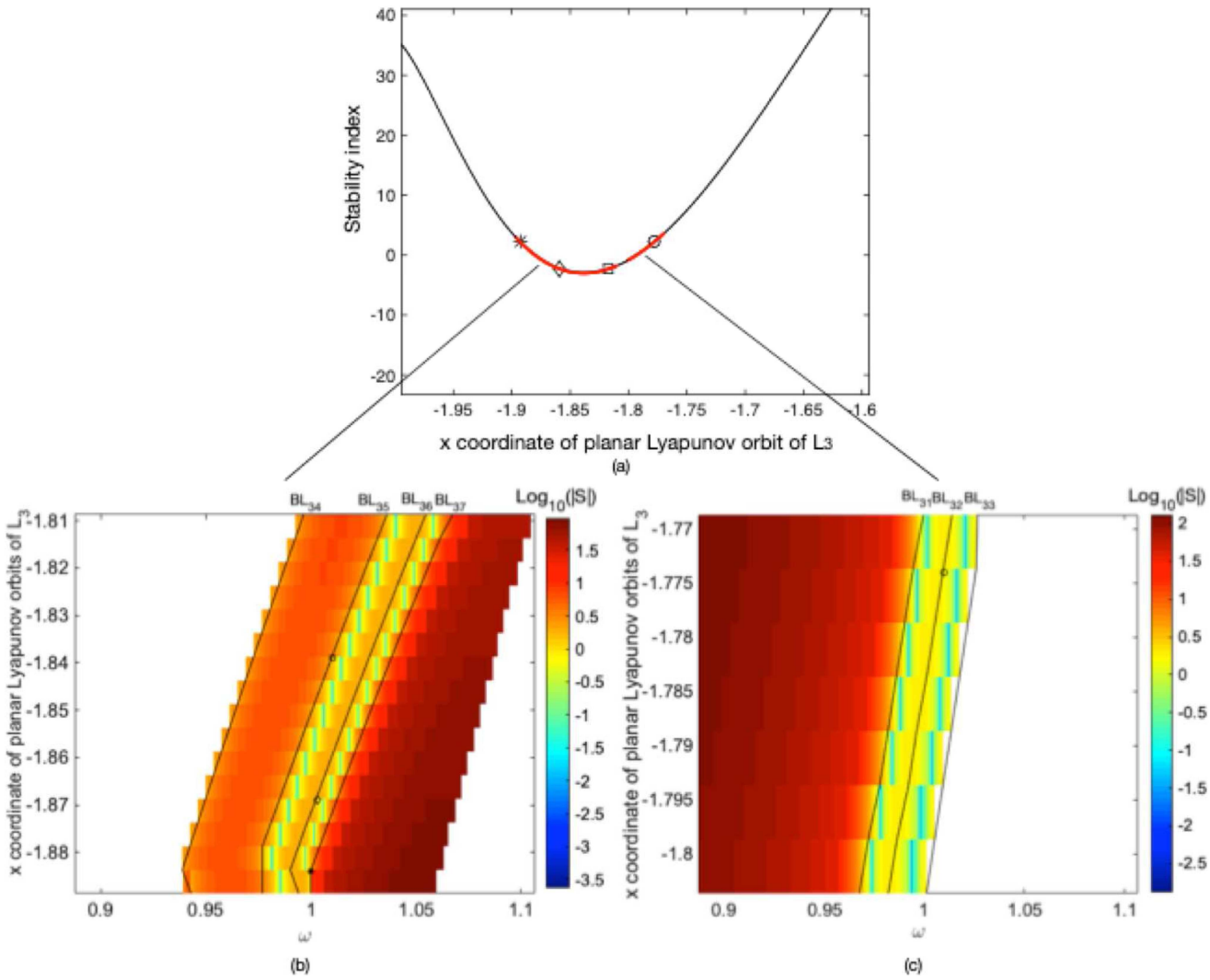

FIG. 10. The bifurcation of the planar Lyapunov orbit family of L_3 as ω varies.

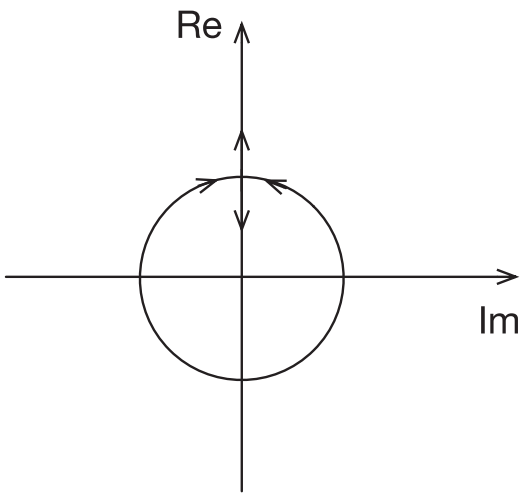

FIG. 11. The routine of eigenvalues across BL_{31}.

The two collinear EPs are of the saddle × center type with one-dimensional stable/unstable manifolds and two-dimensional center manifolds, while the two triangular ones are linearly unstable with two-dimensional stable/unstable manifolds and zero-dimensional center manifolds.

The aforementioned results are obtained in the case of $\omega = 1$ and $\mu = 0.34$. By the LR3BP model used in this paper, the mass distribution of contact binary asteroid systems is highly generalized by the system parameter μ. Another parameter ω is related to the rotation of the binary system. Different from most of the planets in the solar system, some of the asteroids rotate irregularly, such as 2000 PH5 with increasing angular velocity. Thus, taking the value of ω at a specific time as the reference, the normalized angular velocity of these asteroids will have a remarkable increase or decrease from 1 in a short period. According to Eq. (2), the independent parameter ω exert an important effect in the dynamical property of LR3BP, e.g., the existence and the stability of the EPs will change, which suggests the appearance of both static and dynamical bifurcations in the dynamical system.[29]

The existence and the topological structure of the EPs are discussed as $\omega \in (0, 1]$ and $[1, 2]$. As $\omega \to 2$, the angular velocity of the asteroid increases to two times that of the reference state, i.e., $\omega = 1$. $\omega \to 0$ implies that the asteroid gradually stops its rotation. A dramatic change in the dynamical system happens in this extreme case.

Take L_2 as an example to show the static bifurcation of the dynamical system as ω varies. Figure 4 presents the x coordinate of L_2 as $\omega \in (0, 8]$ and the distribution of the eigenvalues is illustrated in Fig. 4(a). As shown in Fig. 4, the x coordinate of L_2 tends to positive infinity as $\omega \to 0^+$ theoretically, implying that such an EP does not exist in reality. In a similar manner, it can be proved that L_3 is located at the negative infinity on the far side of the secondary theoretically as $\omega \to 0^+$, as demonstrated in Fig. 4. The distribution of the four eigenvalues of L_3 is presented in Fig. 5(b). Obviously, if the value of ω is further decreased to any negative number Υ, the location of EPs and their stability are the same as the one in the case of $\omega = -\Upsilon$, since the asteroid system rotates to the negative direction. In summary, according to Fig. 5, the topological type of L_2 and L_3 does not change as ω varies. The static bifurcation occurs as $\omega \to 0^+$, and the collinear EPs disappear at infinity of the x axis.

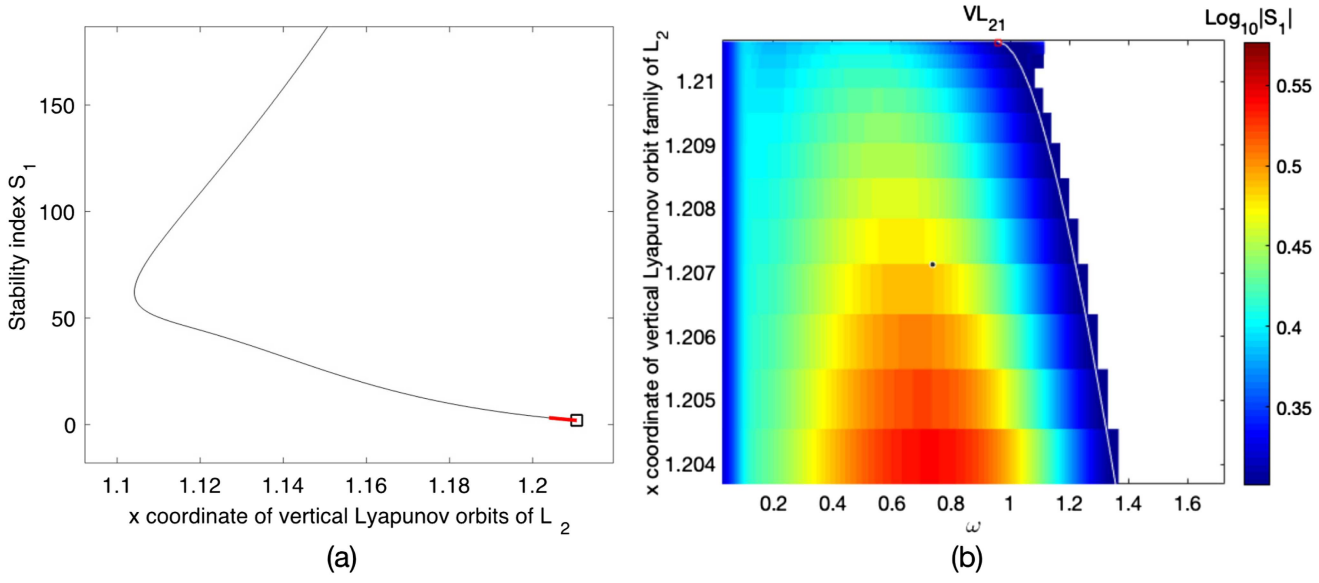

FIG. 12. The bifurcation phenomenon (S_1) of the vertical Lyapunov orbit family of L_2 as ω varies.

Furthermore, the coordinates of the EPs can be deduced from Eq. (2) analytically. Take triangular EP L_4 as an example to discuss the influence of ω in the existence and the stability of L_4 in an analytic way. According to the dynamical definition of the EP, such equations hold at any EP (x, y) that

$$\begin{cases} \frac{\partial \Omega}{\partial x} = 0, \\ \frac{\partial \Omega}{\partial y} = 0, \end{cases} \tag{6}$$

where $\Omega = \omega^2(x^2+y^2)/2 + (1-\mu)/r_1 + \mu/r_2$, and r_1 and r_2 denotes the distance with respect to the primary and the secondary from the EP, respectively. Hence,

$$\begin{cases} \omega^2 y - \frac{1-\mu}{r_1^3} y - \frac{\mu}{r_2^3} y = 0, \\ \omega^2 x - \frac{1-\mu}{r_1^3}(x+\mu) - \frac{\mu}{r_2^3}(x-1+\mu) = 0. \end{cases} \tag{7}$$

For triangular EPs, the y coordinate is nonzero. Substituting $y \neq 0$ into the first equation of Eq. (7) yields

$$\omega^2 - \frac{1-\mu}{r_1^3} - \frac{\mu}{r_2^3} = 0. \tag{8}$$

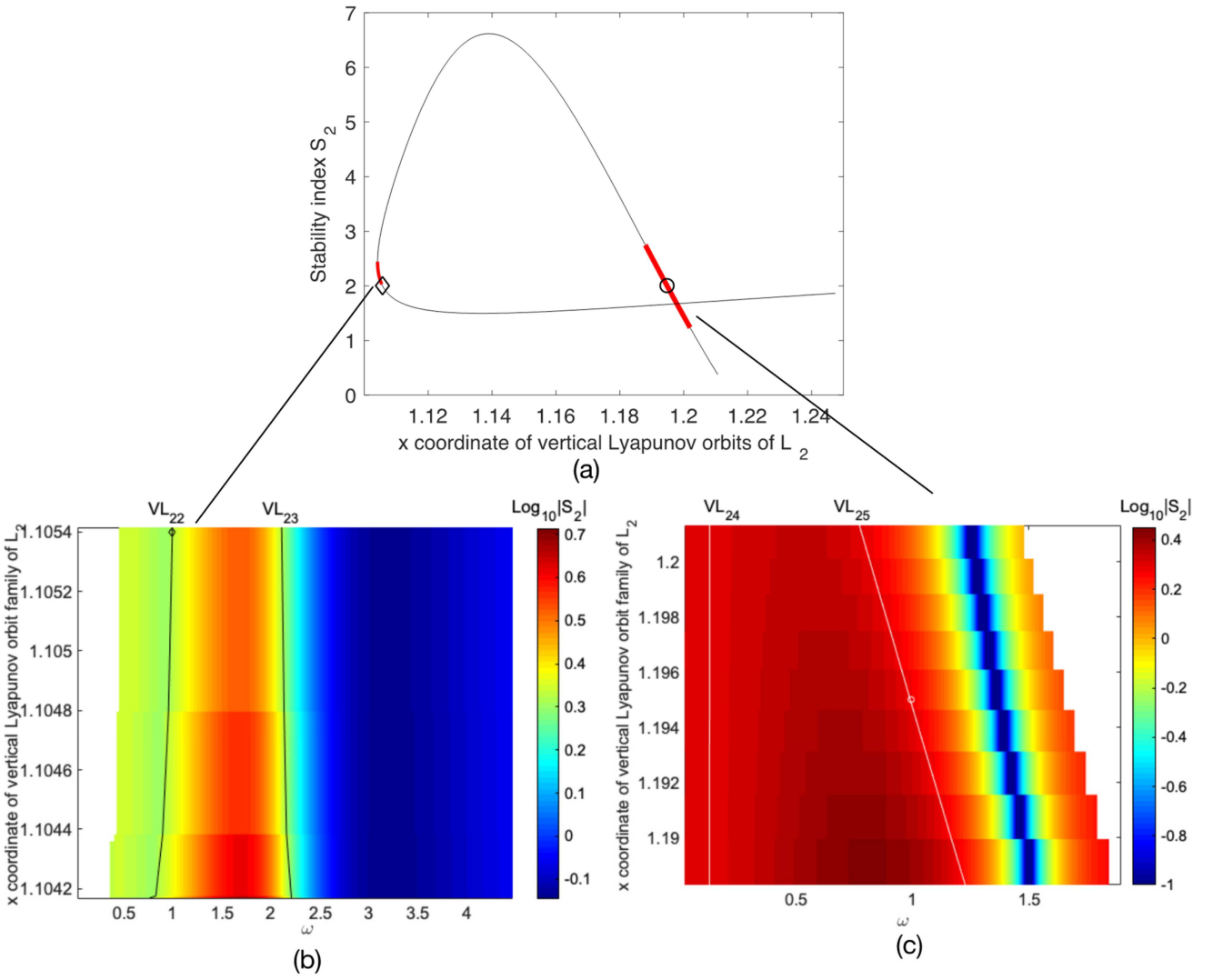

FIG. 13. The bifurcation phenomenon (S_2) of the vertical Lyapunov orbit family of L_2 as ω varies.

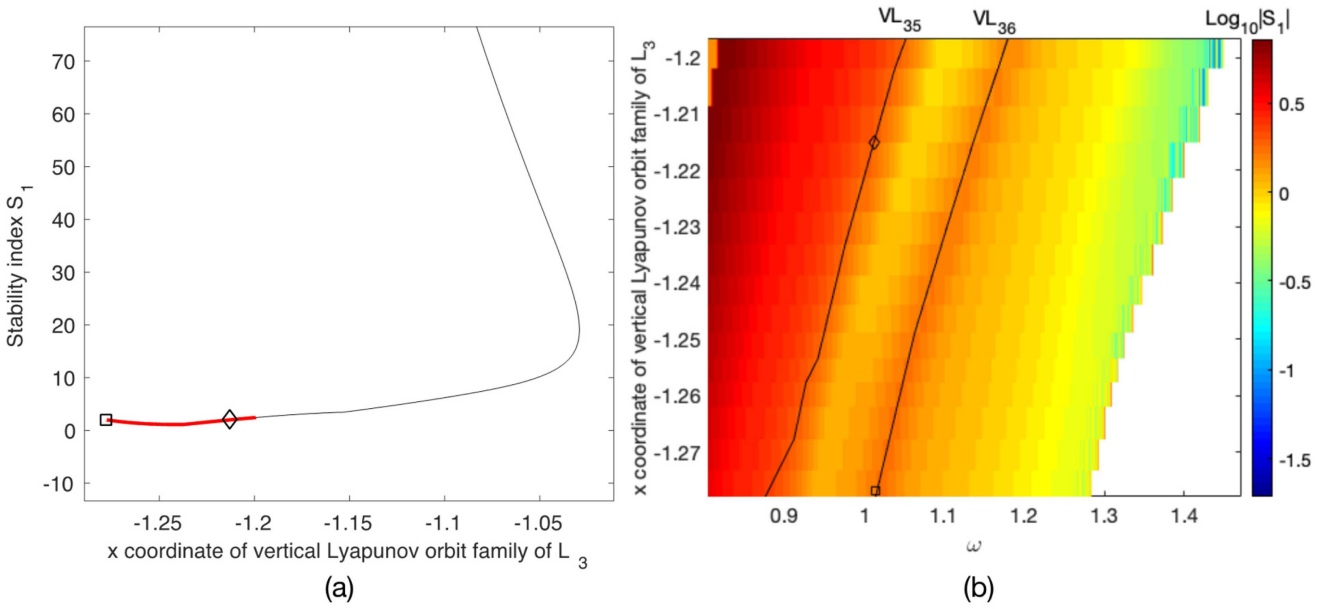

FIG. 14. The bifurcation phenomenon (S_1) of the vertical Lyapunov orbit family of L_3 as ω varies.

Then, substituting Eq. (8) into the second equation of Eq. (7) yields that $r_1 = r_2$. Thus,

$$r_1 = r_2 = \left(\frac{1}{\omega}\right)^{2/3}. \tag{9}$$

According to the normalization of length in LR3BP in Sec. II, the normalized distance between the primary and the secondary is regarded as the unit of length, i.e., 1. Then,

$$r_i \geq 0.5 \quad (i = 1, 2). \tag{10}$$

Substituting into Eq. (9) yields the range of ω as follows:

$$0 < \omega \leq 2\sqrt{2} \cong 2.8284. \tag{11}$$

According to Eq. (9), $r_1 \to \infty$ as $\omega \to 0^+$. Thus, the theoretical location of L_4 is at positive infinity. As ω increases from 0^+, L_4 moves from infinity toward the x axis and ultimately collides with L_1 at $\omega = 2\sqrt{2}$. Once $\omega > 2\sqrt{2}$, the assumption that $y \neq 0$ does not hold. In this case, L_4 is located along the primary-secondary line but coincides with L_1, which is out of our research scope because L_4 is essentially located under the surface of the asteroid. Substituting Eq. (9) into Eq. (4) yields the analytical coordinate of L_4 as $(-\mu + 0.5, \sqrt{(\omega^{-4/3} - 0.25)})$ in the case of $0 < \omega \lesssim 2.8284$. Due to the symmetry of LR3BP, the coordinate of L_5 is symmetrical to the one of L_4 about the x axis with the same topological property.

As declared in Ref. 28, the triangular EPs are linearly unstable as $\omega = 1$ and $\mu = 0.34$ with two-dimensional stable/unstable manifolds and zero-dimensional center manifolds. According to the Center Manifold Theorem,[30] there exist no periodic motions near triangular EPs locally. As demonstrated in Fig. 6, L_4 is of the center × center type topologically as $0 < \omega \approx 0.2131$, and there exist two families of periodic orbits near L_4. In the case of $0.2131 < \omega$, it has the same topological type with the one at $\omega = 1$. At $\omega \approx 0.2131$, the topological type of L_4 alters and thereby a typical pitch-fork bifurcation point appear as shown in Fig. 6. Therefore, the variation of ω determines the topological type of L_4 and L_5, and thereby the existences of local periodic orbits near them. The bifurcation along these two families of periodic orbits near L_4 and L_5 is not discussed in Sec. III because they only exist in a small interval of ω.

Therefore, the static bifurcation occurs as $\omega \to 0^+$, where the triangular EPs disappear at infinity; another bifurcation happens as $\omega \to 2\sqrt{2}$, where L_4 and L_5 come to collision on the primary-secondary line and the number of the EPs in the dynamical system decreases to 2.

In this section, the authors show how the static and dynamical bifurcations of the dynamical system appear due to the varying ω instead of focusing on the stability of EPs in Ref. 16, wherein, static bifurcations are demonstrated by analyzing the existence of solutions to the LR3BP system, which is caused by the collision between the collinear and triangular libration points. A typical pitch-fork bifurcation point is found by discussing the topological type of triangular libration points at different values of ω.

IV. ω-MOTIVATED BIFURCATION OF PERIODIC ORBITS IN LR3BP

Playing a critical role in understanding the dynamical system, the periodic orbits are regarded by Poincaré as the only way to explain the global phase space structure of a nonlinear dynamical system.[31] Therefore, the investigation on the bifurcation of periodic orbits in LR3BP provides the theoretical foundation for further discussion on

the dynamical mechanism of irregularly-rotating asteroids. In a classic CR3BP, due to the saddle × center × center topological type of collinear EPs, the motion in their vicinity can be seen as the composition of two oscillators and some hyperbolic behavior.[32] The oscillations in and orthogonal to $(x-y)$ generate periodic motions known as planar and vertical Lyapunov orbits. For a suitable amplitude, both frequencies become equal, leading to two symmetric branches of spatial periodic orbits called as north and south Halo orbits. Figure 7 presents samples of the aforementioned periodic orbits.

In this section, the bifurcations of planar and vertical Lyapunov orbit families and Halo orbit family are detected via continuation along ω, including obtaining the new types of bifurcations. Then, the new bifurcated orbit family is supplemented to Doedel *et al.*'s bifurcation diagram in CR3BP,[22] establishing a global "skeleton" in LR3BP.

A. Bifurcation of periodic orbits as ω varies

1. Planar Lyapunov orbits

The continuation along ω starts from the member of planar Lyapunov orbit family obtained at $\omega = 1$ in CR3BP. The continuation method is developed based on the idea of Gómez and Mondelo.[26]

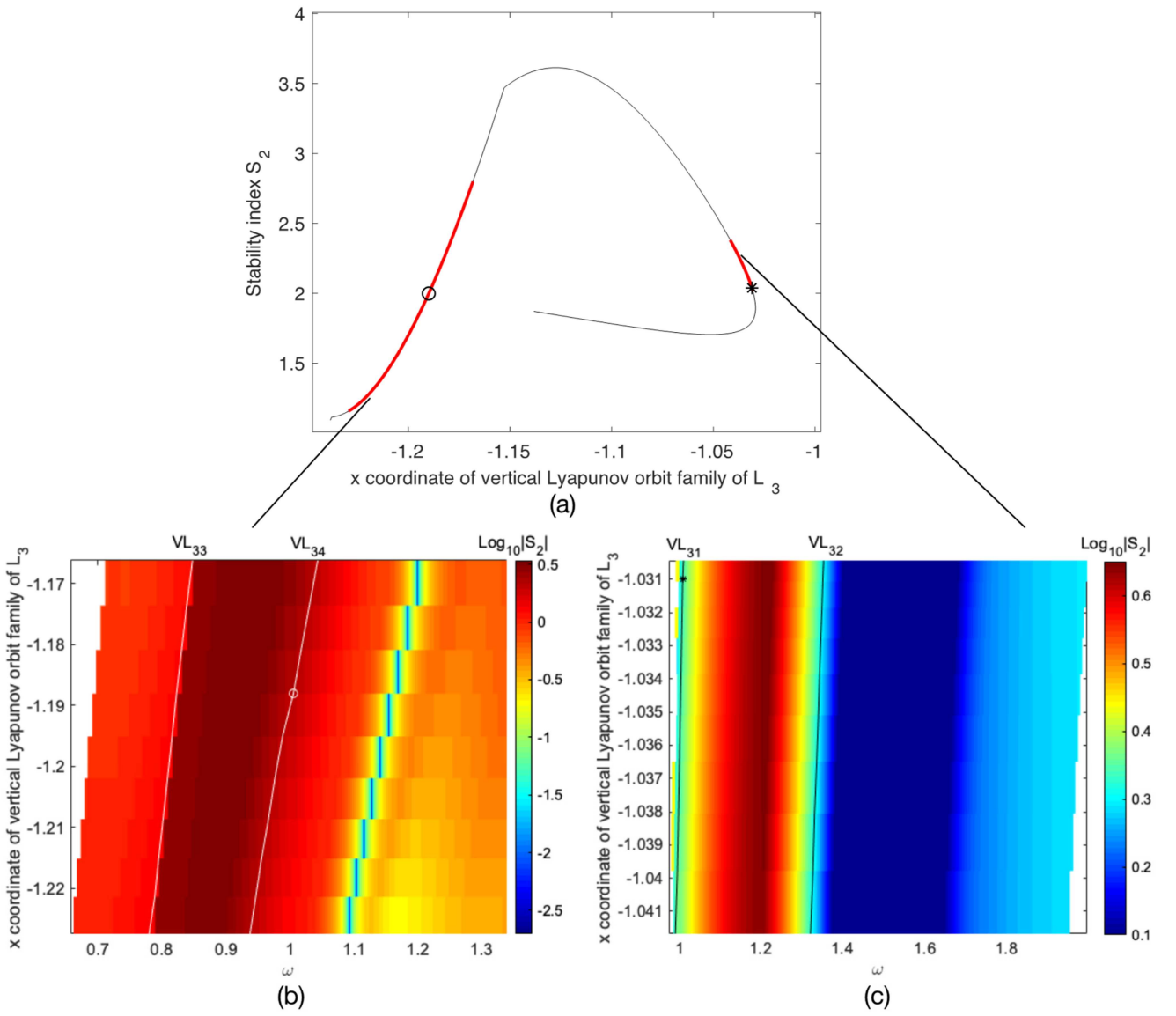

FIG. 15. The bifurcation phenomenon (S_2) of the vertical Lyapunov orbit family of L_3 as ω varies.

In CR3BP, the monodromy matrix $\mathbf{\Lambda}$ of a periodic orbit has such eigenvalues $(1,1, \lambda_1, \lambda_1^{-1}, \lambda_2, \lambda_2^{-1})$.[30] The stability of periodic orbits is indicated by the stability index S_i and $S_i = \lambda_i + 1/\lambda_i$ $(i = 1, 2)$. The eigenvector corresponding to an eigenvalue of 1 indicates the direction of the periodic orbit family, along which such periodicity retains. Except that, there could appear another pair of eigenvalues equal to 1, suggesting another direction of periodicity during the continuation. Potential bifurcation point arises where S_i equals ± 2. Thus, that specific orbit also belongs to another periodic orbit family. However, the bifurcation point must be confirmed by checking their stability change before determined. Note that for planar Lyapunov orbits, only the eigenvalues related to planar motion are taken into consideration, and the corresponding stability index is denoted as S for distinction from the spatial periodic orbits. For vertical Lyapunov orbits and Halo orbits, both S_1 and S_2 are checked.

At $\omega = 1$, there appear two bifurcation points along the planar Lyapunov orbit family of L_2, as presented in Fig. 8(a) by black diamond and square, which represent two tangent bifurcations. The north and south Halo orbit families are generated from the first tangent bifurcation point. From the second tangent bifurcation point, appears the bridge of periodic orbits connecting both the vertical and planar Lyapunov orbit families. In order to explore the ω-motivated bifurcation along this family, two specific intervals containing the tangent bifurcation points are selected from the stability curve, as shown by the red lines in Fig. 8(a). The continuation is implemented starting from each periodic orbit in the selected interval forward and backward in ω. The stability index of each new periodic orbit after continuation is recorded and indicated by the tint of color in Figs. 8(b) and 8(c). The initial state of each planar Lyapunov orbit by continuation can be parameterized as $(x, 0, 0, \dot{y}, \omega)$. The x axis in Fig. 8(a) and the y axis in Figs. 8(b) and 8(c) indicate the x coordinate of its initial state. Similarly, the "x coordinate of vertical Lyapunov orbit or Halo orbit" indicates the x coordinate of the initial state of each vertical Lyapunov orbit or Halo orbit by continuation along ω in the following sections.

Due to the continuity of the LR3BP and the continuation method, the new bifurcation points form a queue instead of scatters, indicated by the black line in Figs. 8(b) and 8(c). The set of bifurcation points in one queue is denoted by BL_{2i} $(i = 1,2,\ldots,7)$, where BL_{21} contains the first tangent bifurcation and BL_{26} contains the second one.

To further discuss the stability change of planar Lyapunov orbits of L_2 under the variation of ω, the eigenvalue distribution near the bifurcation point must be analyzed and concluded. Figure 9 presents the routine of the eigenvalues for periodic orbits across the bifurcation of BL_{22} and BL_{25}. In Fig. 9, the x- and y axes indicate the imaginary and real parts of the eigenvalues for the monodromy matrix of each planar Lyapunov orbit by continuation, respectively. The radius of the central circle is 1. As shown by the arrows in Fig. 9(b), before the bifurcation set BL_{25}, the eigenvalue pair (λ, λ^{-1}) is a pair of conjugate complex numbers with $||\lambda|| = 1$, located on the unit circle in the first and fourth quadrant. As ω increases to 1, this eigenvalue pair approaches to the real positive axis along the unit circle. At the bifurcation point in BL_{25}, the eigenvalue pair come to a collision at the real "1" point and escape to the real positive and negative directions along the y axis after the bifurcation point, respectively. The eigenvalues now are a pair of inverse real numbers. Such an eigenvalue routine indicates a tangent bifurcation.[30] Figure 9(a) presents that the eigenvalue pair comes to a collision at the real "−1" point at the bifurcation point in set BL_{22}, which indicates a period-doubling bifurcation.[30] Therefore, BL_{22} and BL_{25} contain period-doubling and tangent bifurcation points, respectively. The stability of periodic orbits has not altered crossing the bifurcation points in BL_{23}, BL_{24}, and BL_{27}, which is not explored in this paper. Note that only potential bifurcation

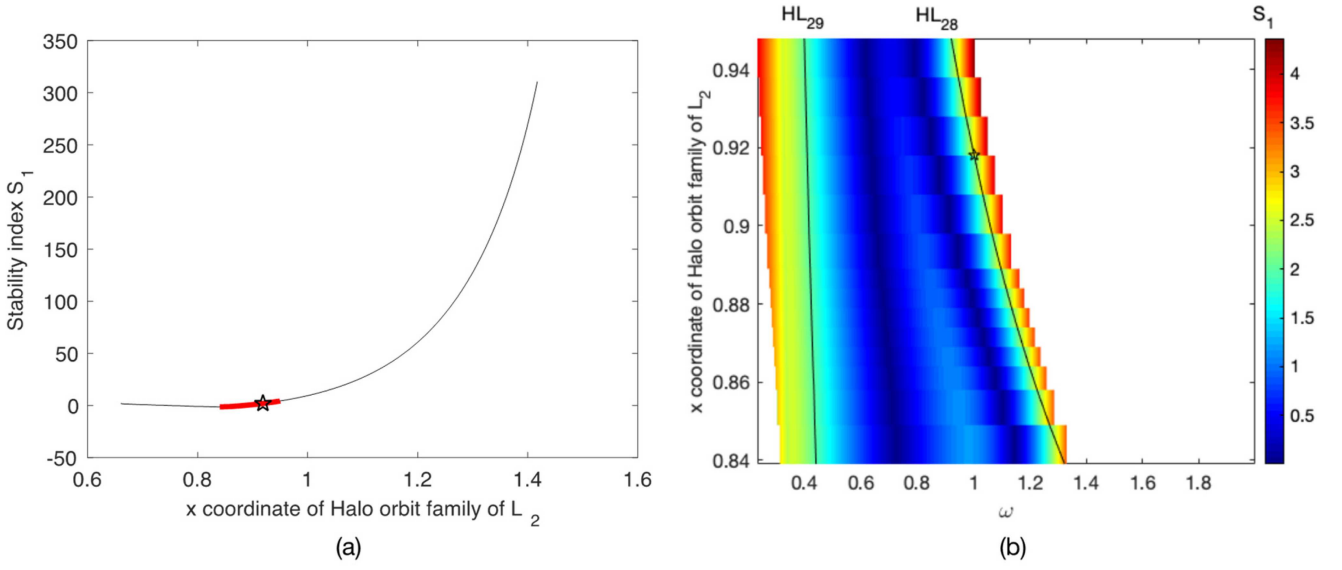

FIG. 16. The bifurcation phenomenon (S_1) of the Halo orbit family of L_2 as ω varies.

points are determined according to the stability index. To check their topological type, eigenvalue routine across the potential bifurcation must be checked. Furthermore, the bifurcated orbits can be constructed analytically by small perturbation or obtained numerically by the Poincaré section.

Subsequently, the bifurcation phenomenon of planar Lyapunov orbit family of L_3 as ω varies can be explored in a similar manner. At $\omega = 1$, there appear four bifurcation points along the planar Lyapunov orbit family of L_3, indicated by a circle, square, diamond, and star in Fig. 10(a), respectively. From the first tangent bifurcation point bifurcated are the north and south branch of Halo orbit families. From the second tangent bifurcation point, emerges the bridge of periodic orbits connecting both the vertical and planar Lyapunov orbit families. The limiting orbit family is generated from the third period-doubling bifurcation point. Select two specific intervals containing these bifurcations from the stability curve and implement the continuation from each periodic orbit of the selected interval forward and backward in ω. Figures 10(b) and 10(c) illustrate the stability index of the new periodic orbits via continuation along the direction of ω increasing and decreasing from 1, denoted as ω^+ and ω^-, respectively. The bifurcation sets are indicated by BL_{3i}, $(i = 1,2,\ldots,7)$, where BL_{32} contains the first period-doubling bifurcation point in Fig. 10(a) and the rest are contained in BL_{35}, BL_{36}, and BL_{37}, respectively. Figure 11 shows the routine of stability index across the bifurcation

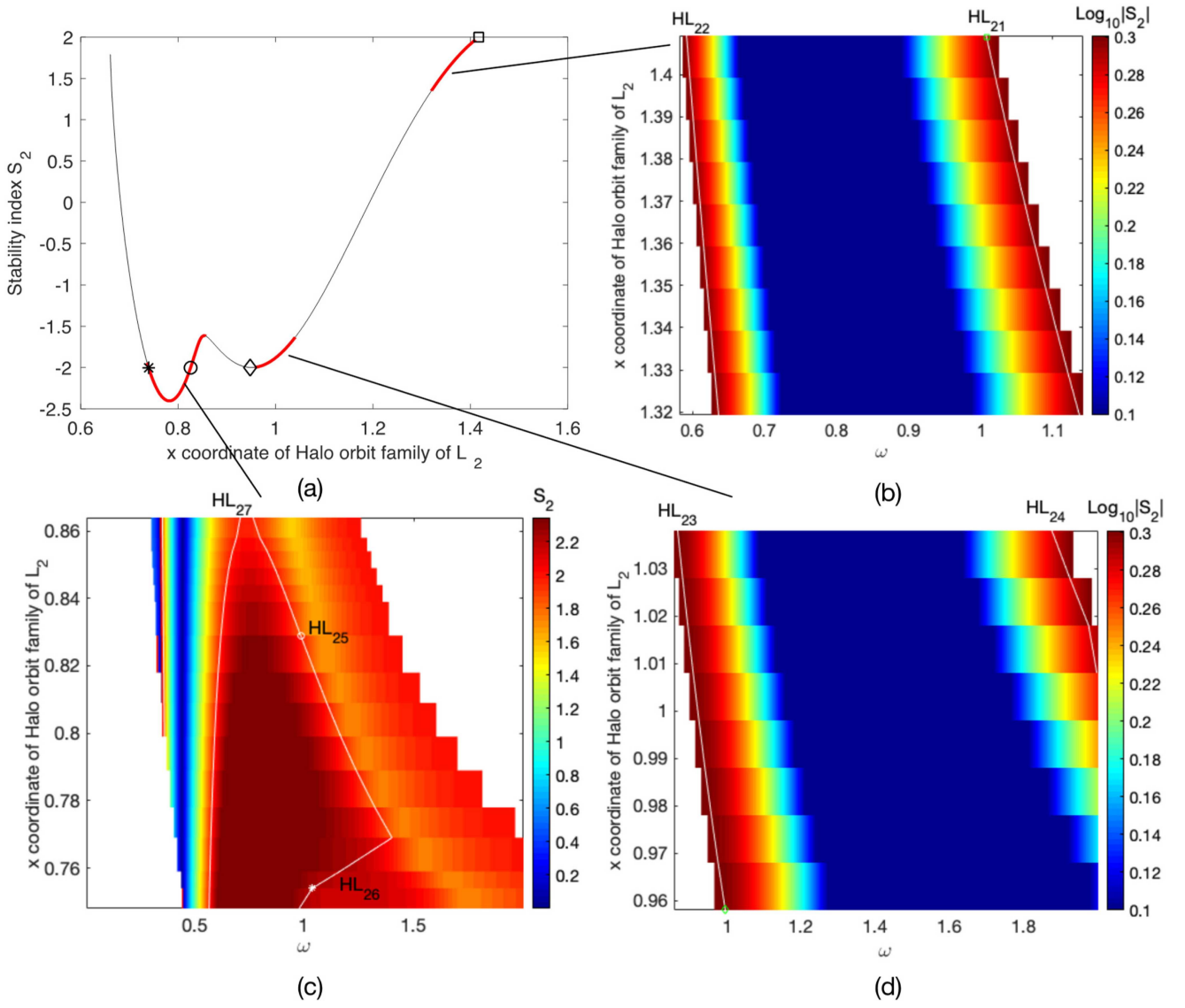

FIG. 17. The bifurcation phenomenon (S_2) of the Halo orbit family of L_2 as ω varies.

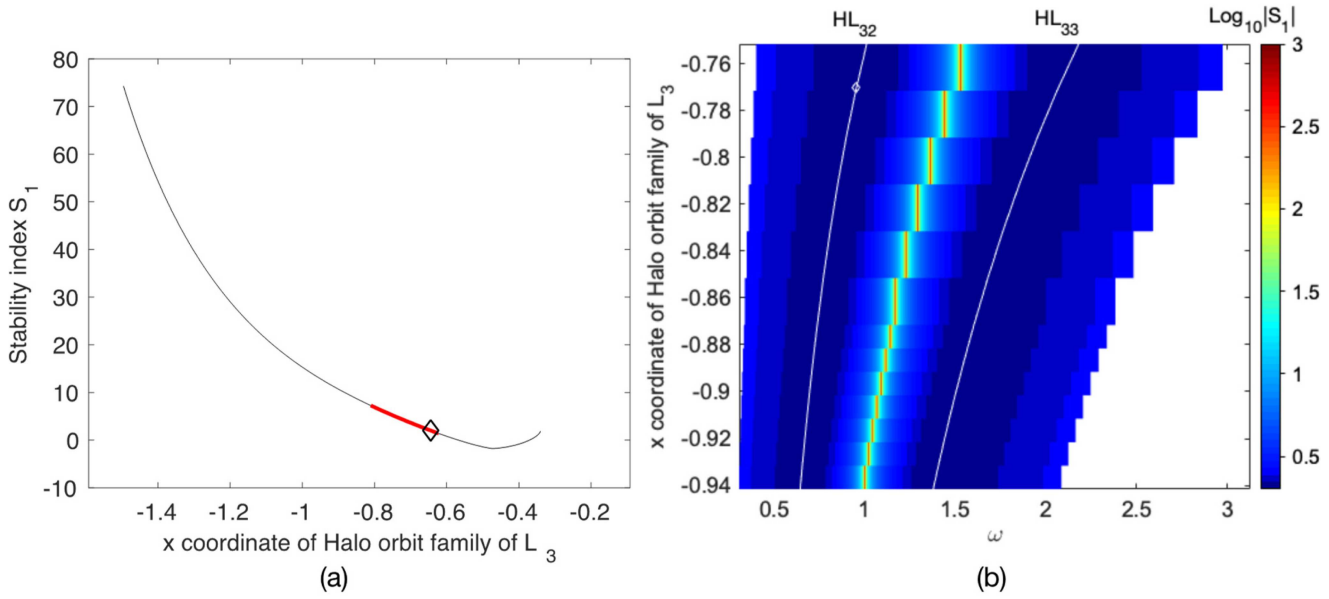

FIG. 18. The bifurcation phenomenon (S_1) of the Halo orbit family of L_3 as ω varies.

points in BL_{31} and demonstrates those are tangent bifurcations. The stability of periodic orbits has not altered crossing the bifurcation of BL_{33} and BL_{34}, and thereby they are not discussed in this paper as well.

2. Vertical Lyapunov orbits

The bifurcation of vertical Lyapunov orbit family is discussed based on two stability indexes S_1 and S_2. According to Gómez and Mondelo,[26] there are three bifurcation points along the vertical Lyapunov orbit family of L_2 at $\omega = 1$, i.e., a period-doubling bifurcation generating a planar periodic orbit around the primary, the secondary and L_3, a tangent bifurcation, and another tangent bifurcation generating the bridge of periodic orbits connecting to the planar Lyapunov orbit family, which are indicated by a square, circle, and diamond in Figs. 12(a) and 13(a), respectively. In a similar manner to the planar Lyapunov orbit family, the bifurcation along ω^+ and ω^- direction is obtained and presented in Figs. 12 and 13. The bifurcation sets are indicated by VL_{2i}, $(i = 1,2,\ldots,5)$, where VL_{21} contains the first period-doubling bifurcation point in Fig. 12(a), and the rest are contained in VL_{25} and VL_{22}, respectively. The routine of the eigenvalues crossing the bifurcation points in VL_{23} and VL_{24} suggests that both of them are of the tangent type. As illustrated in Fig. 13(b), as the contact binary asteroid system spins slowly, i.e., as ω decreases, there appears no new bifurcation points along the periodic orbits, of which the x coordinate locates between 1.204 and 1.214. Particularly, as ω becomes smaller than 0.1, the value of S_1 tends to 2. According to Sec. III, L_2 moves along the primary-secondary line toward the positive infinity in this case. As presented in Fig. 13, in both cases that ω increases or decreases, there occur bifurcations along the periodic orbits, of which the x coordinate locates between 1.1042 and 1.1054. The bifurcation points in VL_{23} are new compared to the vertical Lyapunov orbit family as $\omega = 1$. Further increasing the value of ω to 4, the stability index S_2 gradually decreases but no other new bifurcations appear. Besides, as ω decreases, there occurs a set VL_{24} containing new tangent bifurcation points along the periodic orbits, of which the x coordinate locates between 1.19 and 1.205.

There are four bifurcation points along the vertical Lyapunov orbit family of L_3 at $\omega = 1$, indicated by a square, diamond, circle, and star in Figs. 14(a) and 15(a), respectively. Similar to the ω-motivated bifurcation of the vertical Lyapunov orbit family of L_2, the periodic orbit connecting the planar Lyapunov orbit family of L_3 is bifurcated from the first tangent bifurcation point, and the fourth period-doubling bifurcation point is essentially the termination of the vertical family. However, the second tangent bifurcation generates the vertical periodic orbits of triangular EPs, which is determined by the relevance of the dynamical structure for L_3 and two triangular EPs. Under the variation of ω, the periodic orbits near these bifurcation points are continued to generate the new bifurcation phenomenon, as shown in Figs. 14 and 15. Denote VL_{3i} $(i = 1,2,\ldots,6)$ as a set containing the same type of bifurcation points. VL_{31} and VL_{34} contain the first and second tangent bifurcation points in Fig. 14(a), respectively, while the rest bifurcations belong to the set VL_{35} and VL_{36}. As presented in Fig. 15, as ω decreases, there occur a new bifurcation set VL_{33} along the periodic orbits, of which the x coordinate locates between -1.27 and -1.23. In contrast, another bifurcation set VL_{34} appears along the periodic orbits, of which the x coordinate locates between -1.041 and -1.031 as ω increases.

3. Halo orbits

Different from planar and vertical Lyapunov orbits, Halo orbits do not emerge from oscillation motion near the EP with infinitely

small amplitude. South and north branches of Halo orbits are bifurcated from the planar Lyapunov orbit family. Due to their symmetry, only one branch is studied in this section.

It has been demonstrated by Gómez and Mondelo[26] that there are three period-doubling and two tangent bifurcation points along the Halo orbit family of L_2 and L_3 at $\omega = 1$. Continuation is implemented upon Halo orbits near these five bifurcation points along ω^+ and ω^-. The associated stability index is recorded, as shown in Figs. 16–19. For Halo orbit family of L_2, HL_{2i} $(i = 1,2,\ldots,9)$ is denoted as the set of bifurcation points of the same type and HL_{3i} $(i = 1,2,\ldots,7)$ is denoted as those for the Halo orbit family of L_3. As presented in Fig. 17, the first tangent bifurcation points generating Halo orbits constitutes the set HL_{21}. HL_{23}, HL_{25}, and HL_{26} consisting of three period-doubling bifurcation points, respectively. As ω decreases below 0.7, there appears a new period-doubling bifurcation set HL_{22} along those Halo orbits, of which the x coordinate locates between 1.32 and 1.42. As ω increases to 1.8, another period-doubling bifurcation set HL_{24} occurs by continuation along those Halo orbits, of which the x coordinate locates between 0.96 and 1.04. As presented in Fig. 17(c), as ω increases from 0.2 to 1.8, two period-doubling bifurcation points appear during the continuation of each Halo orbit along ω^+ and ω^- direction, of which the x coordinate locates between 0.75 and 0.86. They belong to set HL_{27} and HL_{25} (or HL_{26}), respectively. Family of the continued orbits from those

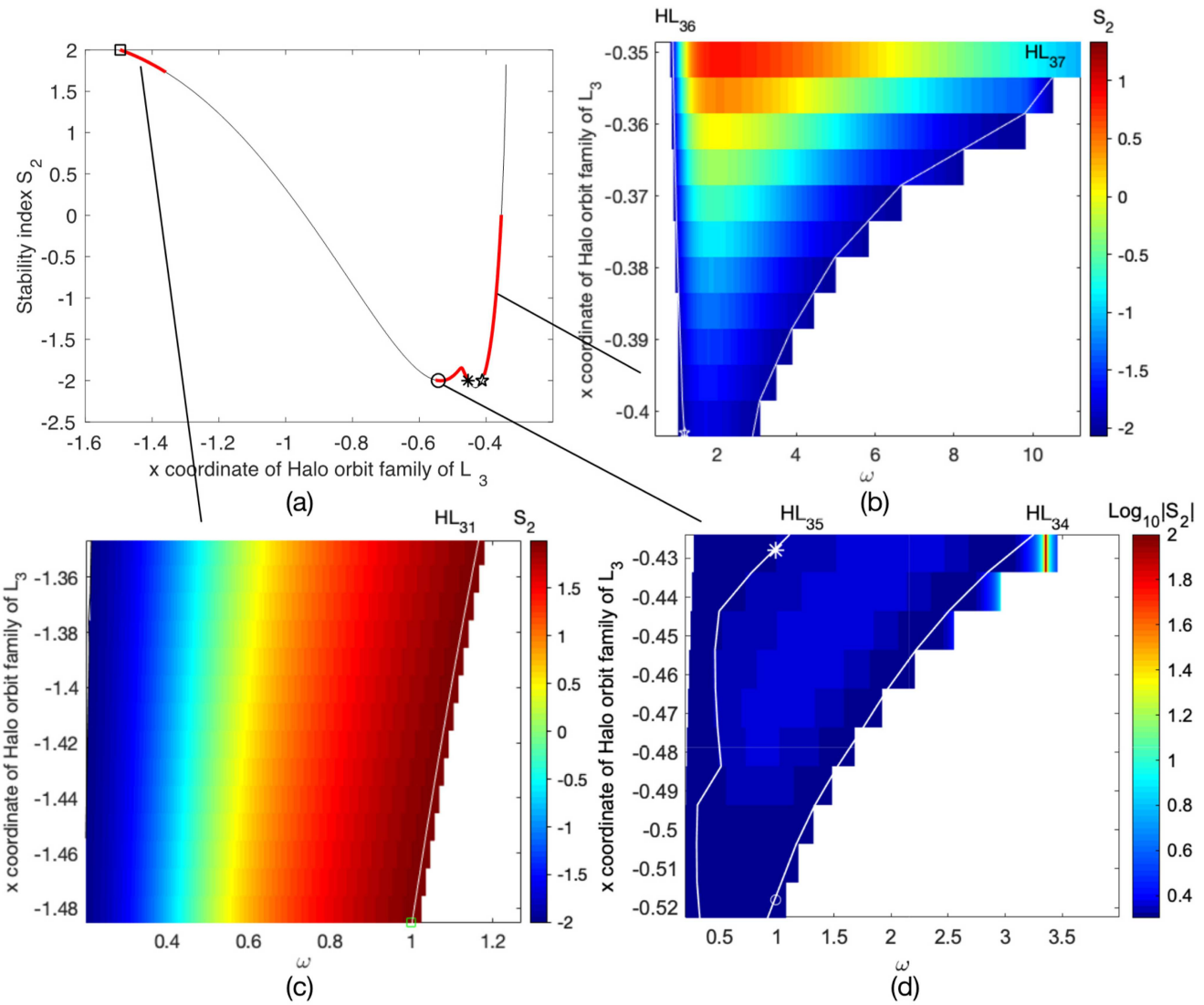

FIG. 19. The bifurcation phenomenon (S_2) of the Halo orbit family of L_3 as ω varies.

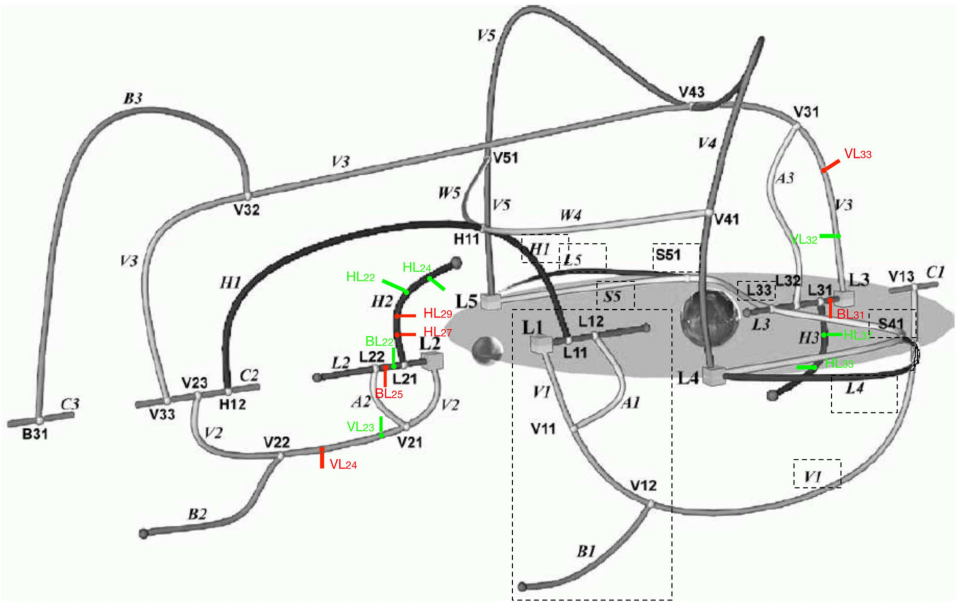

FIG. 20. The global diagram of periodic orbit families and bifurcated families in LR3BP based on Ref. 22.

Halo orbits with x coordinate from 0.76 to 0.86 own two period-doubling bifurcation points, belonging to HL_{25} and HL_{26} respectively, as ω increases from 1.0 to 1.4. The period-doubling bifurcations in HL_{25} and HL_{26} and the corresponding bifurcated families of periodic orbits are presented in Ref. 26 and are not discussed in this paper. Importantly, the lines indicating HL_{25} and HL_{26} intersect with each other at $\omega = 1.4$, suggesting the change of the number of the bifurcation points in the LR3BP and thereby the change of their topological structure. In other words, a special dynamical phenomenon appears in this case, which is named as the "bifurcation of bifurcation" or "secondary bifurcation" in this paper.

Figures 18 and 19 present the bifurcation of Halo orbit family of L_3 with ω varies. The first tangent bifurcation points belong to the set HL_{31}. Denote HL_{34}, HL_{35}, and HL_{36} as sets of three period-doubling bifurcation points along the Halo orbit family of L_3. Particularly, the set HL_{32} contains the fourth tangent bifurcation point during the continuation. The sets containing new period-doubling bifurcation points are denoted by HL_{32} and HL_3. As ω increases from 1, only the continued orbits from those Halo orbits with the x coordinate between -0.81 and -0.63 or -0.405 and -0.305 will own new period-doubling bifurcation points, which constitute the sets HL_{32} and HL_{37}, respectively.

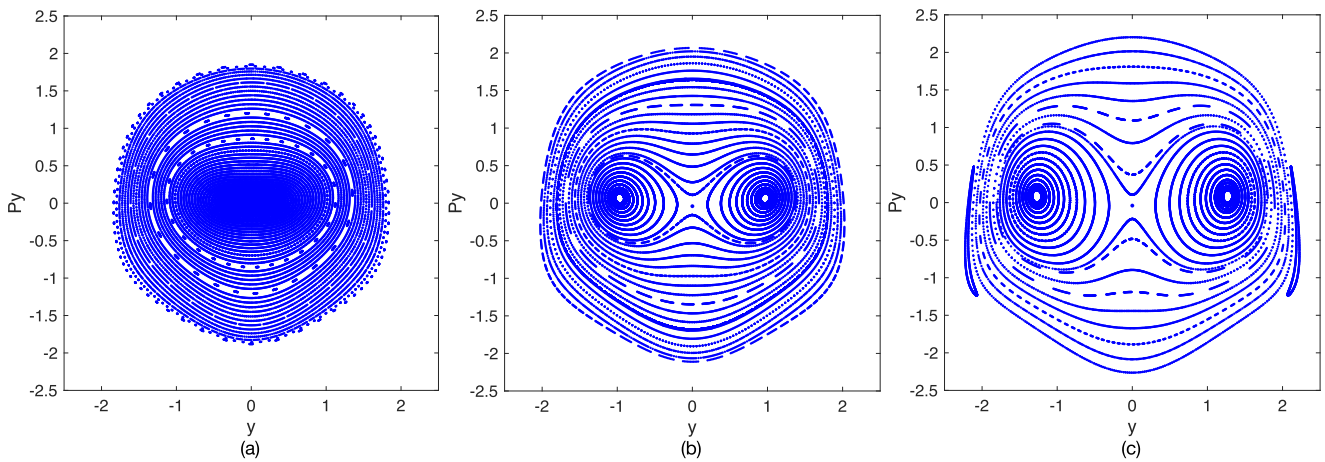

FIG. 21. Poincaré sections of center manifolds of L_2 at $\omega = 1.1$, $h = 3.0$ (a), 4.0 (b), and 5.0 (c).

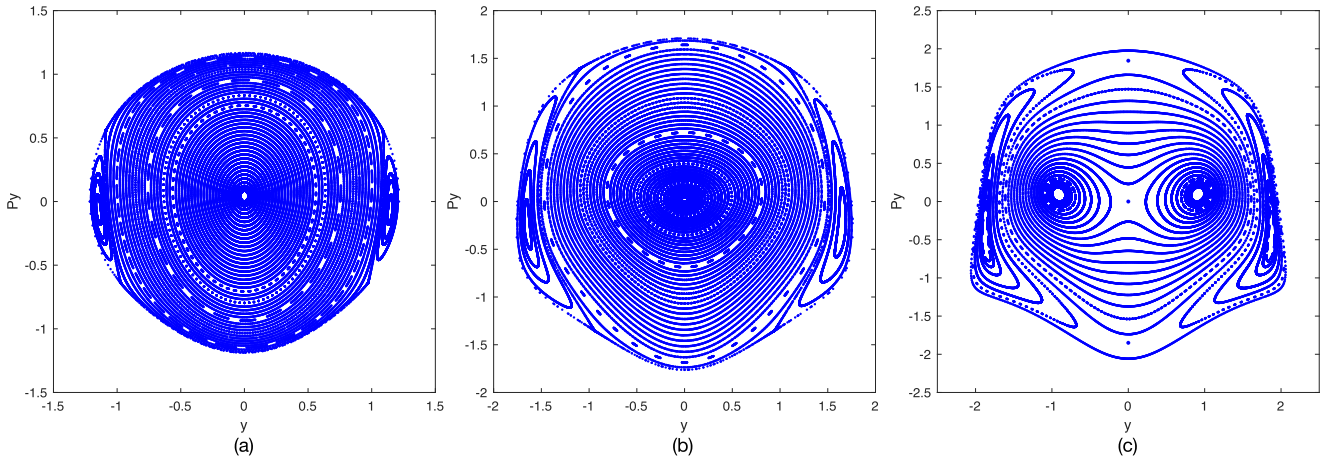

FIG. 22. Poincaré sections of center manifolds of L_2 at $\omega = 1.04$, $h = 1.4$ (a), 3.0 (b), and 4.0 (c).

B. Global diagram of bifurcation in LR3BP

Doedel *et al.* employed the numerical boundary value techniques to obtain a rather complete classification of certain types of periodic solutions of CR3BP, for all values of the mass ratio parameter.[22,23] Furthermore, the bifurcation diagram of CR3BP is presented based on the families that emanate from the EPs, and subsequent families that originate at pitch-fork bifurcation points along the primary branches, as shown in Fig. 20. In this section, the new bifurcation and bifurcated families in the last sections are supplemented to the result of Doedel *et al.*, as illustrated in Fig. 20. Most of the bifurcations and periodic orbit families in CR3BP still exist in LR3BP due to the assumption of LR3BP with the following exceptions: the bifurcation and periodic orbit families associated with L_1 and the planar periodic orbits of triangular EPs. According to the configuration of LR3BP, the L_1 between the primary and the secondary is located under the surface of the celestial body, so the associated branches in Fig. 20 are encircled by dashed lines to distinguish them. Since the results of this paper are obtained in LR3BP at $\mu = 0.34$, the triangular EPs are no longer of the center × center × center type and there locally exists no periodic orbits near them.[33] The associated branches are also encircled by dashed lines. As shown in Fig. 20, the green and red lines indicate the new bifurcated families in LR3BP as ω decreases and increases from 1, respectively, with the same denotation in Secs. IV A. Our results contribute to systematical understanding the distribution of periodic orbit families in LR3BP and to the further investigation on the internal relationship among them. These periodic orbits work as the global "skeleton" in the phase space of LR3BP, guiding future periodic orbits searching in the three-body problem.

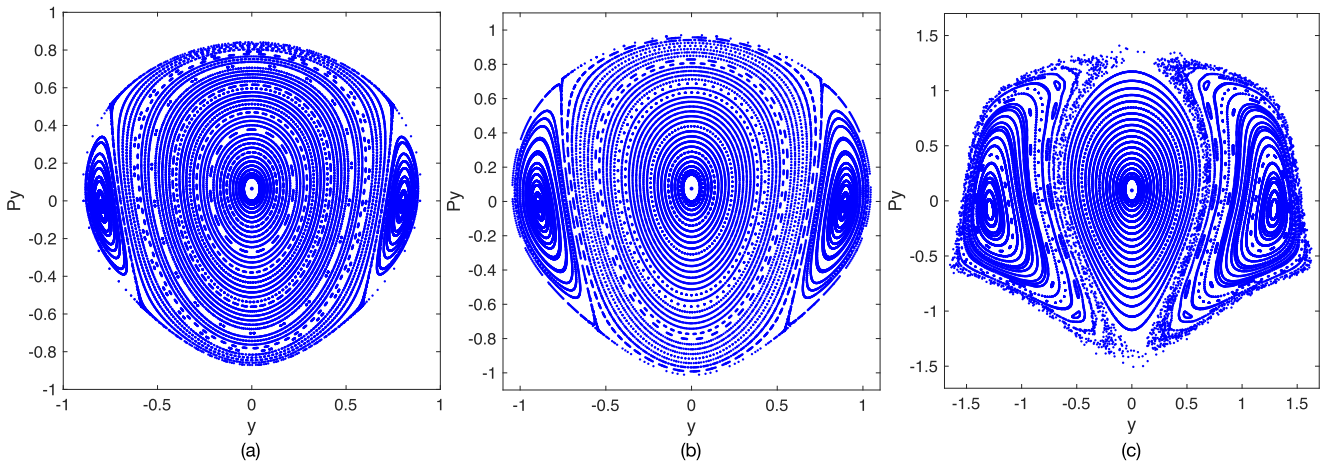

FIG. 23. Poincaré sections of center manifolds of L_2 at $\omega = 0.95$, $h = 0.6$ (a), 0.8 (b), and 1.74 (c).

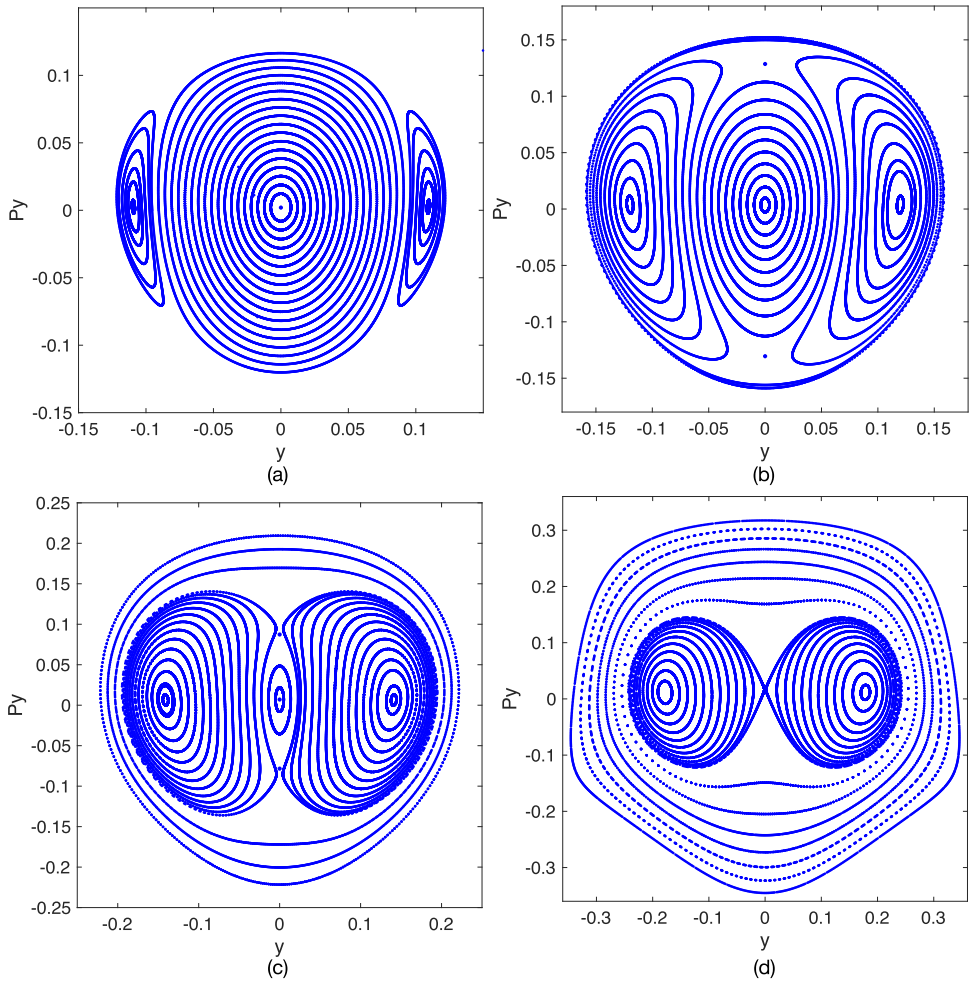

FIG. 24. Poincaré sections of center manifolds of L_3 at $\omega = 0.95$, $h = 0.006$ (a), 0.01 (b), 0.02 (c), and 0.05 (d).

V. C-MOTIVATED BIFURCATION OF PERIODIC ORBITS IN LR3BP

A. Lie series method

By introducing a symplectic transformation

$$\boldsymbol{T}_0 = \begin{bmatrix} 1 & 0 & 0 & 0 \\ 0 & 1 & 0 & 0 \\ 0 & -1 & 1 & 0 \\ 1 & 0 & 0 & 1 \end{bmatrix},$$

a set of Hamiltonian variables are yielded as $[\tilde{x}\,\tilde{y}\,p_{\tilde{x}}\,p_{\tilde{y}}]^T = \boldsymbol{T}_0[\tilde{x}\,\tilde{y}\,\dot{\tilde{x}}\,\dot{\tilde{y}}]^T$ and $p_{\tilde{z}} = \dot{\tilde{z}}$. Hence, Eq. (4) can be written in the Hamiltonian form as

$$\mathcal{H}_2 = \frac{1}{2}(p_{\tilde{x}}^2 + p_{\tilde{y}}^2 + p_{\tilde{z}}^2) + \omega\tilde{y}p_{\tilde{x}} - \omega\tilde{x}p_{\tilde{y}} + \frac{1}{2}(\omega^2 - \Omega_{\tilde{x}\tilde{x}})\tilde{x}^2 + \frac{1}{2}(\omega^2 - \Omega_{\tilde{y}\tilde{y}})\tilde{y}^2 - \frac{1}{2}\Omega_{\tilde{z}\tilde{z}}\tilde{z}^2 + \Omega_{\tilde{x}\tilde{y}}\tilde{x}\tilde{y} \tag{12}$$

Rewrite it into the matrix form as

$$\begin{pmatrix} \dot{\tilde{x}} \\ \dot{\tilde{y}} \\ \dot{\tilde{z}} \\ \dot{p}_{\tilde{x}} \\ \dot{p}_{\tilde{y}} \\ \dot{p}_{\tilde{z}} \end{pmatrix} = \begin{pmatrix} 0 & \omega & 0 & 1 & 0 & 0 \\ -\omega & 0 & 0 & 0 & 1 & 0 \\ 0 & 0 & 0 & 0 & 0 & 1 \\ \Omega_{\tilde{x}\tilde{x}} - \omega^2 & \Omega_{\tilde{x}\tilde{y}} & 0 & 0 & 1 & 0 \\ \Omega_{\tilde{x}\tilde{y}} & \Omega_{\tilde{y}\tilde{y}} - \omega^2 & 0 & -1 & 0 & 0 \\ 0 & 0 & \Omega_{\tilde{z}\tilde{z}} & 0 & 0 & 0 \end{pmatrix} \begin{pmatrix} \tilde{x} \\ \tilde{y} \\ \tilde{z} \\ p_{\tilde{x}} \\ p_{\tilde{y}} \\ p_{\tilde{z}} \end{pmatrix} = \tilde{\boldsymbol{M}} \begin{pmatrix} \tilde{x} \\ \tilde{y} \\ \tilde{z} \\ p_{\tilde{x}} \\ p_{\tilde{y}} \\ p_{\tilde{z}} \end{pmatrix}. \tag{13}$$

Hence, the six eigenvalues λ_j ($j = 1, 2, 3, \ldots, 6$) can be yielded through eigenvalue decomposition upon $\tilde{\boldsymbol{M}}$, and they are one pair of opposite real numbers and two pairs of conjugate pure imaginary numbers, respectively. For simplicity, denote that $\lambda_{3/4} = \pm i\omega_2$ and $\lambda_{5/6} = \pm i\omega_3$ and $\lambda_{1/2} = \pm\omega_1$. The corresponding eigenvectors are denoted by $\boldsymbol{v}_j = \boldsymbol{u}_j + i \cdot \boldsymbol{w}_j$ ($j = 1, 2, 3, \ldots, 6$) and $\boldsymbol{w}_j = \boldsymbol{0}$ for $j = 1$ and 2, where i indicates the unit imaginary number and $\boldsymbol{u}_j$ and $\boldsymbol{w}_j$ denote the real and imaginary parts of $\boldsymbol{v}_j$, respectively.

To normalize the six-dimensional center manifolds, a symplectic transformation $\boldsymbol{T_1}$ is constructed as $[\boldsymbol{u_1}/s_1, \boldsymbol{u_3}/s_2, \boldsymbol{u_5}/s_3, -\boldsymbol{u_1}/s_1, \boldsymbol{w_3}/s_2, \boldsymbol{w_5}/s_3]^T$, where $s_1 = \omega_1^5 + 2\Omega_{\tilde{x}\tilde{x}}\omega_1^3 + (\Omega_{\tilde{x}\tilde{x}} + 1)(\Omega_{\tilde{x}\tilde{x}} - 3)\omega_1$, $s_2 = \omega_2^5 + 2\Omega_{\tilde{x}\tilde{x}}\omega_2^3 + (\Omega_{\tilde{x}\tilde{x}} + 1)(\Omega_{\tilde{x}\tilde{x}} - 3)\omega_2$ and $s_3 = \sqrt{\omega_3}$. By $\boldsymbol{T_1}$, Eq. (12) is cast into

$$\mathcal{H}_2 = \omega_1 \tilde{x} p_{\tilde{x}} + \frac{\omega_2}{2}(p_{\tilde{y}}^2 + \tilde{y}^2) + \frac{\omega_3}{2}(p_{\tilde{z}}^2 + \tilde{z}^2), \tag{14}$$

which can be further put into the following complex normal form:

$$\mathcal{H}_2 = \omega_1 q_1 p_1 + \sqrt{-1}\omega_2 q_2 p_2 + \sqrt{-1}\omega_3 q_3 p_3 \tag{15}$$

by adding a symplectic transformation

$$T_2 = \begin{bmatrix} \frac{1}{\sqrt{2}} I_{2\times 2} & \frac{-i}{\sqrt{2}} I_{2\times 2} \\ \frac{-i}{\sqrt{2}} I_{2\times 2} & \frac{1}{\sqrt{2}} I_{2\times 2} \end{bmatrix}$$

to $[\tilde{y}, \tilde{z}, p_{\tilde{y}}, p_{\tilde{z}}]$.

As shown in Sec. III, the topological type of the EPs L_2 and L_3 has not altered as ω varies. Hence, the reduction to center manifolds is accomplished in a similar manner by the method developed by Jorba and Masdemont,[25] the dynamics near the collinear EPs can be qualitatively described as a combination of hyperbolic motion and invariant manifolds tangent to two central directions, respectively, by Eq. (15). To eliminate the effect of the hyperbolic motion, a Lie series method will be implemented upon the high-order terms of Hamiltonian function $\mathcal{H}$ as follows:

$$\mathcal{H}(q,\ p) = \mathcal{H}_2(q,\ p) + \sum\nolimits_{n\geq 3} \mathcal{H}_n(q,\ p), \tag{16}$$

where $\mathcal{H}_2$ is given in Eq. (15). Given a Hamiltonian generation function $\mathcal{G}(q, p)$, a function $\hat{\mathcal{H}}$ defined as

$$\hat{\mathcal{H}} \equiv \mathcal{H} + \{\mathcal{H}, \mathcal{G}\} + \frac{1}{2!}\{\{\mathcal{H}, \mathcal{G}\}, \mathcal{G}\} + \frac{1}{3!}\{\{\{\mathcal{H}, \mathcal{G}\}, \mathcal{G}\}, \mathcal{G}\} + \cdots \tag{17}$$

is the result of applying a canonical change to $\mathcal{H}$. Then, to eliminate the monomials of degree 3 of Eq. (16), a generation function of a homogeneous polynomial of degree 3 defined as $\mathcal{G}_3$ is built up such that $\{\mathcal{H}_2, \mathcal{G}_3\} = -\mathcal{H}_3$. Denote that

$$\begin{aligned} \mathcal{H}_3(q,p) &= \sum\nolimits_{|k_q|+|k_p|=3} h_{k_q,k_p} q^{k_q} p^{k_p}, \mathcal{G}_3(q,p) \\ &= \sum\nolimits_{|k_q|+|k_p|=3} g_{k_q,k_p} q^{k_q} p^{k_p} \text{ and } \mathcal{H}_2(q,p) = \sum\nolimits_{j=1}^{3} \eta_j q_j p_j. \end{aligned}$$

So, it is easy to obtain

$$\mathcal{G}_3 = \sum\nolimits_{|k_q|+|k_p|=3} \frac{-h_{k_q,k_p}}{\langle k_p - k_q,\ \eta\rangle} q^{k_q} p^{k_p}, \quad \eta = (\omega_1,\ i\omega_2, i\omega_3). \tag{18}$$

Similarly, a generation function $\mathcal{G}_4$ of degree 4 can be constructed and used to obtain the change corresponding to the fourth order of the Hamiltonian function. Furthermore, the Hamiltonian function can be normalized to any required order by performing $\mathcal{G}_5$, $\mathcal{G}_6$, etc. The detailed information on the normalization of a Hamiltonian function and the construction of a generation function can be found in Refs. 25–27.

B. Bifurcation of periodic orbits as *C* varies

By means of numerical integration, the dynamical flow of the reduced Hamiltonian $\mathcal{H}(\tilde{y}, p_{\tilde{y}}, \tilde{z}, p_{\tilde{z}})$ after normalization is truncated by the Poincaré section $\{\Sigma_1 : \tilde{z} = 0, p_{\tilde{z}} > 0\}$. Note that after the normalization, the value of the Hamiltonian function is denoted by h, which plays an equivalent role as the Jacobi energy C and thereby is adopted to quantify the energy level of center manifolds in this section. Figures 21–23 present the C-motivated bifurcation of periodic orbits of L_2 with different angular velocities and those of L_3 in Figs. 24 and 25.

The analysis on the C-motivated bifurcation phenomena in LR3BP is achieved through a comparison with the case at $\omega = 1$ in CR3BP and among cases at different energy levels. The basic structure is inherited from the results of Jorba and Masdemont[25] and Gómez and Mondelo,[26] where the outer curve indicates the planar Lyapunov orbit together with its torus, and the center fixed point indicates the vertical Lyapunov orbits. As the energy increases, the south and north branches of Halo orbit families emerge from the bifurcation of planar Lyapunov orbits, indicated by two symmetrical invariant tori in Fig. 21(c) and in subfigures of Figs. 22–25. The boundary between the torus of the Halo orbit and the torus around the vertical Lyapunov orbit is a homoclinic trajectory of the planar Lyapunov orbit.

Furthermore, the authors will demonstrate that the angular velocity exerts an important effect on the dynamical behavior near collinear EPs of LR3BP by stimulating some specific bifurcations of CR3BP. Each invariant torus surrounding the center fixed point corresponds to a Lissajous orbit. The evolution of this structure depends on the value of ω and selected EPs. One pattern is presented in Figs. 22–25, where it shrinks to the inner part under the expansion of the invariant tori of Halo orbits as the energy changes, even disappear at the center point as shown in Figs. 25(d) and 24(d). It has been detected and discussed in detail in Refs. 25 and 26. However, in some cases, this structure still remains until chaotic motions appear as the energy increases, as shown in Figs. 22 and 23. Besides, as illustrated in Fig. 21, two branches of periodic orbits and their quasiperiodic orbits are bifurcated from the vertical Lyapunov orbit. The associated invariant torus emerges from the fixed center point, whose torus is stretched outwards the outer curve as the energy varies. The first pattern is named as "shrinking-vanishing mode," while the second and the last patterns are called "shrinking-existing mode" and "stretching mode," respectively, which represents the unique dynamical phenomenon at a specific value of ω in LR3BP. It is very significant to point out that the area between the tori of Halo orbits and vertical Lyapunov orbit is not blank but at least contains the trace of invariant manifolds of planar Lyapunov orbits.

Looking into the region close to the invariant torus of vertical Lyapunov orbit, two additional fixed points are located on the $y = 0$ axis, as shown in Figs. 22(c), 24(b), 24(c), 25(c), and 25(d). They represent two periodic orbits, each one in a different lane of a bridge connecting the planar and the vertical Lyapunov families, as described in Sec. IV A. Particularly, in Figs. 24 and 25, it can be found that at small energy values, two lanes of connecting orbits start from a bifurcation point of the planar Lyapunov orbit family. As energy increases, they move along the $y = 0$ axis toward the center fixed point until colliding with each other. Meanwhile, the center torus vanishes,

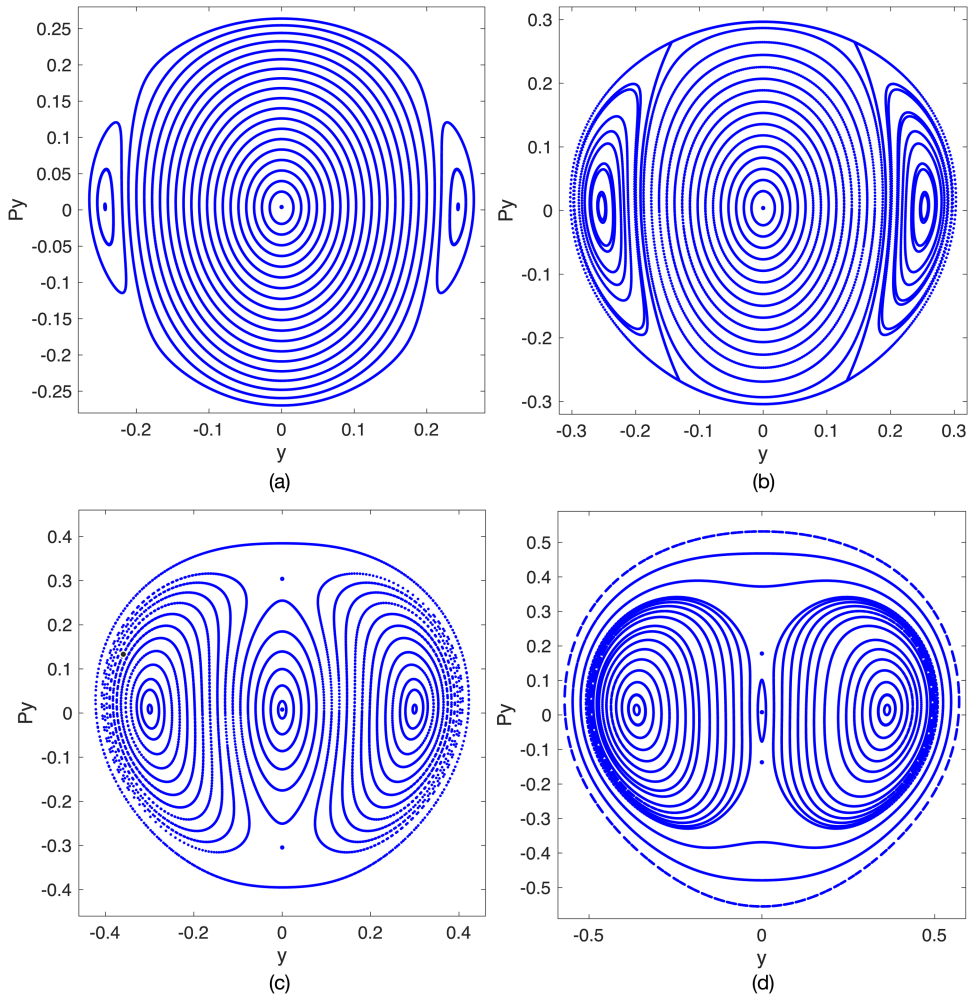

FIG. 25. Poincaré sections of center manifolds of L_3 at $\omega = 1.1$, $h = 0.04$ (a), 0.05 (b), 0.1 (c), and 0.18 (d).

indicating the vertical Lyapunov orbit alters from stable to unstable and two lanes terminate at this bifurcation of the vertical family.

Another unique phenomenon compared with CR3BP is presented in Figs. 21 and 22, where two symmetric tori emerge from a torus of the center fixed point before the bifurcation of Halo orbits. They correspond to two stable periodic orbits bifurcated from the vertical Lyapunov orbit as energy increases. With their emerging, the stability of the vertical Lyapunov orbit alters from stable to unstable. The region between these two tori and the invariant tori surrounding them is filled with the trace of the invariant manifolds of unstable vertical Lyapunov orbits. These two symmetric periodic orbits belong to a special family of periodic orbits emerging from a period-doubling bifurcation, which is named as elliptic bifurcation by period duplication in the work of Gómez and Mondelo.[26]

Besides, Fig. 23 demonstrates that the evolution of center manifolds of L_2 at $\omega = 0.95$ follows the rule showed in CR3BP.[26] Nevertheless, as the value of energy indicator h increases to 1.74, the most outer curve breaks up into chaotic scatters, indicating the collision of the planar Lyapunov orbit with the secondary in LR3BP. Meanwhile, the chaotic motion arises before the Lie series method reaches its convergence radius and even before the torus of vertical Lyapunov orbit vanishes.

VI. CONCLUSION

This paper focuses on the bifurcation of a linked restricted three-body problem (LR3BP), especially the discovery of new bifurcation under the variation of angular velocity ω and Jacobi energy C with a fixed mass ratio μ. Targeting at a kind of irregularly-rotating asteroids, the LR3BP is emerged from the classic circular restricted three-body problem (CR3BP) given that the primary and the secondary is physically linked.

First, the bifurcation of equilibrium points (EPs) in LR3BP is studied by detecting their existence analytically and analysing their

topological types numerically. The results show a dramatic change of the EPs number as $\omega \to 2\sqrt{2}$ or 0. The topological type of triangular EPs alters from linearly unstable to stable center × center at $\omega \approx 0.2131$. Subsequently, the influence of ω in the bifurcation of periodic orbits of collinear EPs is explored numerically by continuation upon planar and vertical Lyapunov orbit families and Halo orbit family along ω^+ and ω^- directions. Not only new bifurcation points are obtained but also a unique dynamical phenomenon is demonstrated, which is called the "bifurcation of bifurcation" or "secondary bifurcation." Next, the detected new bifurcated families are supplemented to the result of Doedel *et al.*,[22,23] obtaining a global bifurcation diagram in the context of LR3BP.

Finally, to explore the C-motivated bifurcations, the phase space structures near collinear EPs are revealed numerically by a reduction to center manifolds through the Lie series method at a selected value of ω. The basic structures of the center manifolds presented on the Poincaré section of LR3BP are inherited from those in CR3BP while some unique dynamical behaviors are discovered. The evolution of invariant torus of vertical Lyapunov orbit as C changes follows three different patterns, i.e., "shrinking-vanishing mode," "shrinking-existing mode," and "stretching mode." The fixed points, corresponding to the connection orbits of the planar and the vertical Lyapunov families, move along the $y = 0$ axis and collide with the center fixed point as C increases, indicating the vertical Lyapunov orbit alters from stable to unstable and two lanes terminate at this bifurcation of vertical family. At $\omega = 1.1$, before the emerging of Halo orbits, two stable periodic orbits are bifurcated from the vertical Lyapunov orbit of L_2 with energy increasing, which is first detected in this investigation. Besides, as C increases, the most outer curve is torn apart to chaotic scatters before the Lie series method reaches its convergence radius.

In summary, the bifurcation phenomena of LR3BP explored in two dimensions, i.e., ω and C, is not only a very important supplement to classic three-body problem theory mathematically but also provides new insights into orbital dynamics near irregularly-rotating asteroids.

ACKNOWLEDGMENTS

This work was supported by the National Natural Science Foundations of China (NNSFC) (Nos. 11432001 and 11772024), the Fundamental Research Funds for the Central Universities (No. YWF-16-BJ-Y-10), and the Natural Sciences and Engineering Research Council of Canada (NSERC).

REFERENCES

[1] L. Euler, *Theoria Motuum Lunae* (Typis Academiae Imperialis Scientiarum, Petropoli, 1772).
[2] J. L. Lagrange, "Essai sur le probleme des trois corps," Prix de L'académie Royale des Sciences de Paris **9**, 292 (1772).
[3] M. Ceccaroni, A. Celletti, and G. Pucacco, "Halo orbits around the collinear points of the restricted three-body problem," Physica D **317**, 28–42 (2016).
[4] W. S. Koon, M. W. Lo, J. E. Marsden, and S. D. Ross, "Heteroclinic connections between periodic orbits and resonance transitions in celestial mechanics," Chaos **10**, 427–469 (2000).
[5] E. Lega and M. Guzzo, "Three-dimensional representations of the tube manifolds of the planar restricted three-body problem," Physica D **325**, 41–52 (2016).
[6] C. G. Schroer and E. Ott, "Targeting in Hamiltonian systems that have mixed regular/chaotic phase spaces," Chaos **7**, 512–519 (1997).
[7] A. Celletti, F. Paita, and G. Pucacco, "The dynamics of Laplace-like resonances," Chaos **29**, 033111 (2019).
[8] M. Lara, J. F. San-Juan, and S. Ferrer, "Secular motion around synchronously orbiting planetary satellites," Chaos **15**, 043101 (2005).
[9] R. Roncoli and K. Fujii, "Mission design overview for the gravity recovery and interior laboratory (GRAIL) mission," in *AIAA/AAS Astrodynamics Specialist Conference, Toronto, Ontario, 2–5 August 2010* (AIAA, 2010), AIAA-20108383.
[10] K. Uesugi, "Results of the MUSES-A "HITEN" mission," Adv. Space Res. **18**, 69–72 (1996).
[11] V. Szebehely, *Theory of Orbits* (Academic Press, New York, 1967), pp. 8–9.
[12] P. A. Taylor, J. L. Margot, D. Vokrouhlický *et al.*, "Spin rate of asteroid (54509) 2000 PH5 increasing due to the YORP effect," Science **316**, 274–277 (2007).
[13] A. Deprit and A. Deprit-Bartholomé, "Stability of the triangular Lagrangian points," Astronaut J. **72**, 173–179 (1967).
[14] A. P. Markeev, "On the stability of the triangular libration points in the circular bounded three-body problem," J. Appl. Math. Mech. **33**, 112–116 (1969).
[15] S. V. Chermnykh, "Stability of libration points in a gravitational field," Vest Leningrad Univ. 1, 73–77 (1987).
[16] K. Goździewski and A. J. Maciejewsky, "Nonlinear stability of the Lagrangian libration points in the Chermnykh problem," Celest. Mech. Dynam. Astron. **70**, 41–58 (1998).
[17] K. E. Papadakis, "The 3D restricted three-body problem under angular velocity variation," Astron. Astrophys. **425**, 1133–1142 (2004).
[18] E. A. Perdios and O. Ragos, "Asymptotic and periodic motion around collinear equilibria in Chermnykh's problem," Astron. Astrophys. **414**, 361–371 (2004).
[19] X. Wang, J. Li, and S. Gong, "Bifurcation of equilibrium points in the potential field of asteroid 101955 bennu," Mon. Not. Roy. Astron. Soc. **455**, 3724–3734 (2015).
[20] Y. Jiang and X. Liu, "Equilibria and orbits around asteroid using the polyhedral model," New. Astron. **69**, 8–20 (2019).
[21] Y. Jiang, H. Baoyin, X. Wang *et al.*, "Stability and motion around equilibrium points in the rotating plane-symmetric potential field," Results Phys. **10**, 487–497 (2018).
[22] E. J. Doedel, D. J. Dichmann, J. Galan-Vioque *et al.*, "Elemental periodic orbits of the CR3BP: A brief selection of computational results," in *EQUADIFF 2003 International Conference on Differential Equations* (EQUADIFF, 2005), pp. 163–168.
[23] E. J. Doedel, V. A. Romanov, R. C. Paffenroth *et al.*, "Elemental periodic orbits associated with the libration points in the circular restricted 3-body problem," Int. J. Bifurc. Chaos **17**, 2625–2677 (2007).
[24] A. Deprit, "Canonical transformations depending on a small parameter," Celest. Mech. **1**, 12–30 (1969).
[25] A. Jorba and J. Masdemont, "Dynamics in the center manifold of the collinear points of the restricted three body problem," Physica D **132**, 189–213 (1999).
[26] G. Gómez and J. M. Mondelo, "The dynamics around the collinear equilibrium points of the RTBP," Physica D **157**, 283–321 (2001).
[27] T. Luo, M. Xu, and Y. Dong, "Dynamics in the controlled center manifolds by Hamiltonian structure-preserving stabilization," Chaos Soliton Fractal **112**, 149–158 (2018).
[28] Y. Liang, M. Xu, and S. Xu, "Homoclinic/heteroclinic connections of equilibria and periodic orbits of contact binary asteroids," J. Guid. Control. Dynam. **40**, 2042–2061 (2017).
[29] Q. Lu, *Qualitative Methods and Bifurcations of Ordinary Differential Equations* (Beijing University of Aeronautics and Astronautics Press, 2009), pp. 228–238 (in Chinese).
[30] S. Wiggins, *Introduction to Applied Nonlinear Dynamical Systems and Chaos* (Springer-Verlag, Berlin, 2003), Chap. 3.
[31] H. Poincaré, *Les Méthodes Nouvelles de la Mécanique Céleste* (Gauthier-Villars, 1899).
[32] M. Belló M, G. Gómez, and J. J. Masdemont, *Invariant Manifolds, Lagrangian Trajectories and Space Mission Design* (Springer, New York, 2010), pp. 5–7.
[33] Y. Liang, M. Xu, and S. Xu, "High-order solutions of motion near triangular libration points for arbitrary value of μ," Nonlinear Dyn. **93**, 909–932 (2018).